Solution Structures and Dynamic Properties of Chelated d^0 Metal Olefin Complexes $\{\eta^5\text{: }\eta^1\text{-}C_5R_4SiMe_2N^tBu\}Ti(OCMe_2CH_2CH_2CH{=}CH_2)^+$ (R = H, Me): Models for the $\{\eta^5\text{: }\eta^1\text{-}C_5R_4SiMe_2N^tBu\}Ti(R')(olefin)^+$ Intermediates in "Constrained Geometry" Catalysts

Jean-François Carpentier,[†] Vladimir P. Maryin,[†] Jeffrey Luci,[†] and Richard F. Jordan*[,§]

Contribution from the Department of Chemistry, The University of Iowa, Iowa City, Iowa 52242, and Department of Chemistry, The University of Chicago, 5735 S. Ellis Ave., Chicago, IL 60637

Received August 29, 2000

Abstract: To model the Ti−olefin interaction in the putative $\{\eta^5\text{: }\eta^1\text{-}C_5R_4SiMe_2N^tBu\}Ti(R')(olefin)^+$ intermediates in "constrained geometry" Ti-catalyzed olefin polymerization, chelated alkoxide olefin complexes $\{\eta^5\text{: }\eta^1\text{-}C_5R_4SiMe_2N^tBu\}Ti(OCMe_2CH_2CH_2CH{=}CH_2)^+$ have been investigated. The reaction of $\{\eta^5\text{: }\eta^1\text{-}C_5R_4SiMe_2N^tBu\}TiMe_2$ (**1a**,**b**; R = H, Me) with $HOCMe_2CH_2CH_2CH{=}CH_2$ yields mixtures of $\{\eta^5\text{-}C_5R_4SiMe_2NH^tBu\}TiMe_2(OCMe_2CH_2CH_2CH{=}CH_2)$ (**2a**,**b**) and $\{\eta^5\text{: }\eta^1\text{-}C_5R_4SiMe_2N^tBu\}TiMe(OCMe_2CH_2CH_2CH{=}CH_2)$ (**3a**,**b**). The reaction of **2a**/**3a** and **2b**/**3b** mixtures with $B(C_6F_5)_3$ yields the chelated olefin complexes $[\{\eta^5\text{: }\eta^1\text{-}C_5R_4SiMe_2N^tBu\}Ti(OCMe_2CH_2CH_2CH{=}CH_2)][MeB(C_6F_5)_3]$ (**4a**,**b**; 71 and 89% NMR yield). The reaction of **2b**/**3b** with $[Ph_3C][B(C_6F_5)_4]$ yields $[\{\eta^5\text{: }\eta^1\text{-}C_5Me_4SiMe_2N^tBu\}Ti(OCMe_2CH_2CH_2CH{=}CH_2)][B(C_6F_5)_4]$ (**5b**, 88% NMR yield). NMR studies establish that **4a**,**b** and **5b** exist as mixtures of diastereomers (isomer ratios: **4a**/**4a′**, 62/38; **4b**/**4b′**, 75/25; **5b**/**5b′**, 75/25), which differ in the enantioface of the olefin that is coordinated. NMR data for these d^0 metal olefin complexes show that the olefin coordinates to Ti in an unsymmetrical fashion primarily through C_{term} such that the C=C π bond is polarized with positive charge buildup on C_{int}. Dynamic NMR studies show that **4b**/**4b′** undergoes olefin face exchange by a dissociative mechanism which is accompanied by fast inversion of configuration at Ti ("O-shift") in the olefin-dissociated intermediate. The activation parameters for the conversion of **4b** to **4b′** (i.e., **4b**/**4b′** face exchange) are: $\Delta H^{\ddagger}$ = 17.2(8) kcal/mol; $\Delta S^{\ddagger}$ = 8(1) eu. **4a**/**4a′** also undergoes olefin face exchange but with a lower barrier ($\Delta H^{\ddagger}$ = 12.2(9) kcal/mol; $\Delta S^{\ddagger}$ = −2(3) eu), for the conversion of **4a** to **4a′**.

Introduction

Chain growth in insertion polymerization of olefins by early transition metal catalysts involves generation of coordinatively unsaturated, d^0 L_nMR alkyl species, coordination of monomer to form transient $L_nM(R)(olefin)$ alkyl olefin adducts, and migratory insertion.[1] A principal chain transfer reaction, β-H transfer to metal, generates transient $L_nM(H)(olefin)$ hydride olefin adducts which undergo olefin dissociation or displacement. These reactions are illustrated in simplified form in Scheme 1. Understanding the properties of d^0 metal olefin complexes and in particular how the metal−olefin bonding is influenced by the steric and electronic characteristics of the L_nM unit, may provide insights that are useful for the design and application of new catalysts. However, d^0 metal olefin complexes are rare and little is known about their structures, bonding or dynamic properties. Olefins coordinate weakly to d^0 metal centers due to the absence of conventional d-π* back-bonding.[2]

Scheme 1

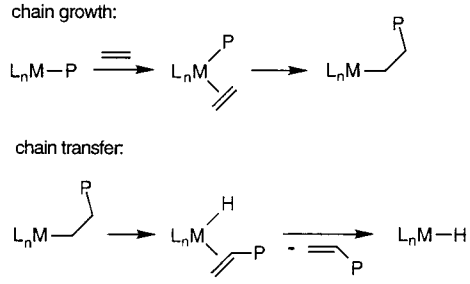

We have developed a simple strategy for the generation of d^0 metal olefin complexes that is based on the use of the flexible alkoxide−olefin ligand $-OCMe_2CH_2CH_2CH{=}CH_2$.[3] Alkyl abstraction from $L_nM(R)(OCMe_2CH_2CH_2CH{=}CH_2)$ complexes generates cationic $L_nM(OCMe_2CH_2CH_2CH{=}CH_2)^+$ species which adopt chelated M−olefin-bonded structures if weakly

* Address correspondence to this author at The University of Chicago.
[†] The University of Iowa.
[§] The University of Chicago.

(1) For reviews concerning olefin polymerization by well-defined early metal catalysts see: (a) Jordan, R. F. *Adv. Organomet. Chem.* **1991**, *32*, 325. (b) Brintzinger, H. H.; Fischer, D.; Mülhaupt, R.; Rieger, B.; Waymouth, R. M. *Angew. Chem., Int. Ed. Engl.* **1995**, *34*, 1143. (c) Bochmann, M. *J. Chem. Soc., Dalton Trans.* **1996**, 255. (d) Kaminsky, W.; Arndt, M. *Adv. Polym. Sci.* **1997**, *127*, 143. (e) Resconi, L.; Cavallo, L.; Fait, A.; Piemontesi, F. *Chem. Rev.* **2000**, *100*, 1253. (f) Chen, E. Y.; Marks, T. J. *Chem. Rev.* **2000**, *100*, 1391.

(2) For a review on metal−olefin bonding, see: Mingos, D. M. P. In *Comprehensive Organometallic Chemistry, 1st* ed.; Wilkinson, G., Stone, F. G. A., Abel, E. W., Eds.; Pergamon: New York, 1982; Vol. 3, p 1.

(3) (a) Carpentier, J.-F.; Wu, Z.; Lee, C. W.; Strömberg, S.; Christopher, J. N.; Jordan, R. F. *J. Am. Chem. Soc.* **2000**, *122*, 7750. (b) Wu, Z.; Jordan, R. F.; Petersen, J. L. *J. Am. Chem. Soc.* **1995**, *117*, 5867.

10.1021/ja003209l CCC: $20.00
Published on Web 01/09/2001

Chart 1

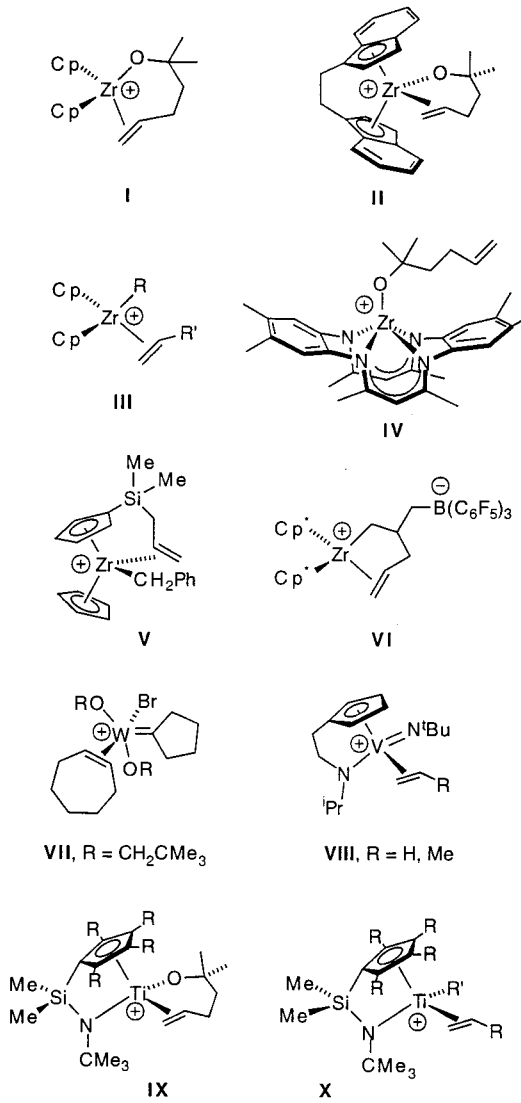

coordinating anions are used and the metal center is sufficiently Lewis acidic to bind the olefin. In an initial study we investigated the metallocene complexes $Cp_2Zr(OCMe_2CH_2CH_2$-$CH{=}CH_2)^+$ (**I**, Cp = C_5H_5) and *rac*-(EBI)$Zr(OCMe_2CH_2CH_2$-$CH{=}CH_2)^+$ (**II**, EBI = ethylene-1,2-bis(1-indenyl)), which are models for the corresponding $(C_5R_5)_2Zr(R)(\alpha$-olefin$)^+$ active species in metallocene catalysis (**III**, Chart 1). Complexes **I** and **II** adopt chelated structures in the solid state and in chlorocarbon solution. The Zr−olefin bonding in these species is unsymmetrical and consists of a weak $Zr-C_{term}$ interaction and minimal $Zr-C_{int}$ interaction. The Zr−olefin bonding does not perturb the structure of the coordinated olefin unit significantly but does polarize the C=C bond such that positive charge is delocalized from Zr to C_{int}. Similar unsymmetrical bonding and polarization effects may contribute to the high insertion reactivity of nonchelated $(C_5R_5)_2Zr(R)(olefin)^+$ species. Dynamic NMR studies show that **I** and **II** undergo olefin face exchange (i.e., exchange of the olefin enantioface that is coordinated to Zr) in solution. The free energy barrier at 298 K for face exchange for **II** ($\Delta G^{\ddagger}_{FE} = 15.3(7)$ kcal/mol) is significantly greater than that for **I** ($\Delta G^{\ddagger}_{FE} = 11.1(8)$ kcal/mol). The face exchange of **II** involves rate-limiting olefin dissociation and fast inversion of configuration at Zr ("O-shift") in the olefin-dissociated intermediate. The difference in the face-exchange barriers of **I** and **II** may reflect differences in Zr−olefin bond strengths, solvent participation in the olefin dissociation, or steric inhibition of chelate ring opening between the two cases. In contrast, cation **IV**, which contains the ancillary N_4-donor ligand octamethyldibenzotetraazaannulene (Me_8taa^{2-}), does not adopt a chelated structure.[4] The absence of olefin coordination in **IV** may reflect the lower Lewis acidity and harder character of the (Me_8taa)-$Zr(OR)^+$ cation as compared to $(C_5R_5)_2Zr(OR)^+$ cations.

Several other chelated olefin complexes of d^0 bent metallocenes have been described.[5] Royo generated **V** by benzyl abstraction from $Cp(\eta^5$-$C_5H_4SiMe_2CH_2CH{=}CH_2)Zr(CH_2Ph)_2$, and Casey prepared **VI** by reaction of the metallacyclobutane complex $Cp^*_2Zr\{CH_2CH(CH_2CH{=}CH_2)CH_2\}$ ($Cp^* = C_5Me_5$) with $B(C_6F_5)_3$ (Chart 1).[6,7] NMR data for **V** and **VI** are consistent with unsymmetrical Zr−olefin bonding similar to that in **I** and **II**, and dynamic NMR studies establish that the free energy barriers to olefin face exchange for **V** (11.7 kcal/mol, includes inversion of configuration at Zr) and **VI** (10.5 kcal/mol) are similar to that observed for **I**. Neutral $Cp^*_2YCH_2CH_2$-$CRR'CH{=}CH_2$ (R, R′ = H, Me) species exhibit weak unsymmetrical bonding of the pendant olefin.[8] Simple, nonchelated d^0 metal olefin complexes are extremely rare, being limited to the W^{VI} cycloheptene adduct **VII**, which is stable below ca. −25 °C, and the V^V ethylene and propylene complexes **VIII**, which have been characterized by NMR.[9,10]

An important current goal in this area is to determine if the properties of nonmetallocene d^0 olefin complexes are similar to those of the metallocene species described above. Here we report studies of $\{\eta^5{:}\eta^1$-$C_5R_4SiMe_2N^tBu\}Ti(OCMe_2CH_2CH_2$-$CH{=}CH_2)^+$ species (**IX**), which are models for the putative $\{\eta^5{:}\eta^1$-$C_5R_4SiMe_2N^tBu\}Ti(R')(olefin)^+$ intermediates (**X**) in the recently developed "constrained geometry" catalyst systems.[11−13] The constrained geometry catalysts have gained technological importance because of their utility in the synthesis of new copolymers of ethylene with α-olefins, styrene, and even isobutylene, and their stability at high polymerization temperatures. A 12-electron $\{C_5R_4SiMe_2NR\}TiX^+$ species is more

(4) Martin, A.; Uhrhammer, R.; Gardner, T. G.; Jordan, R. F.; Rogers, R. D. *Organometallics* **1998**, *17*, 382

(5) (a) Horton, A. D.; Orpen, A. G. *Organometallics* **1992**, *11*, 8. (b) Ahlers, W.; Erker, G.; Fröhlich, R. *Eur. J. Inorg. Chem.* **1998**, 889. (c) Karl, J.; Erker, G. *J. Mol. Catal. A: Chem.* **1998**, *128*, 858. (d) Temme, B.; Karl, J.; Erker, G. *Chem. Eur. J.* **1996**, *2*, 919. (e) Ruwwe, J.; Erker, G.; Fröhlich, R. *Angew. Chem., Int. Ed. Engl.* **1996**, *35*, 80. (f) Erker, G.; Noe, R.; Krüger, C.; Werner, R. *Organometallics* **1992**, *11*, 4174.

(6) Galakhov, M. V.; Heinz, G.; Royo, P. *J. Chem. Soc., Chem. Commun.* **1998**, 17.

(7) Casey, C. P.; Carpenetti, D. W.; Sakuri, H. *J. Am. Chem. Soc.* **1999**, *121*, 9483.

(8) (a) Casey, C. P.; Hallenbeck, S. L.; Pollock, D. W.; Landis, C. R. *J. Am. Chem. Soc.* **1995**, *117*, 9770. (b) Casey, C. P.; Hallenbeck. S. L.; Wright, J. M.; Landis, C. R. *J. Am. Chem. Soc.* **1997**, *119*, 9681. (c) Casey, C. P.; Fagan, M. A.; Hallenbeck, S. L. *Organometallics* **1998**, *17*, 287.

(9) Kress, J.; Osborn, J. A. *Angew. Chem., Int. Ed. Engl.* **1992**, *31*, 1585.

(10) (a) Witte, P. T.; Meetsma, A.; Hessen, B. *J. Am. Chem. Soc.* **1997**, *119*, 10561. (b) Several cationic Nb(V) olefin complexes were recently characterized by NMR. Humphries, M. J.; Douthwaite, R. E.; Green, M. L. H *J. Chem. Soc., Dalton Trans.* **2000**, 2952.

(11) (a) Stevens, J. C.; Timmers, F. J.; Rosen, G.; Knight, G. W.; Lai, S. Y. (Dow Chemical Co.). Eur. Pat. Appl. EP 0416815 A2, 1991. (b) Canich, J. A. (Exxon Chemical Co.) European Patent Application, EP 0420436 A1, 1991. (c) Stevens, J. C. In *Studies in Surface Science and Catalysis*; Soga, K., Terano, M., Eds.; Elsevier: Amsterdam, 1994; Vol. 89, pp 277−284. (d) Stevens, J. C. In *Studies in Surface Science and Catalysis*; Hightower, J. W., Delglass, W. N., Iglesia, E., Bell, A. T., Eds.; Elsevier: Amsterdam, 1996; Vol. 101, pp 11−20. (e) Devore, D. D.; Timmers, F. J.; Hasha, D. L.; Marks, T. J.; Deck, P. A.; Stern, C. L. *Organometallics* **1995**, *14*, 3132.

(12) For the initial design of this ligand system, see: (a) Shapiro, P. J.; Bunel, E.; Schaefer, W. P.; Bercaw, J. E. *Organometallics* **1990**, *9*, 867. (b) Piers, W. E.; Shapiro, P. J.; Bunel, E.; Bercaw, J. E. *Synlett* **1990**, *2*, 74. (c) Shapiro, P. J.; Cotter, W. D.; Schaefer, W. P.; Labinger, J. A.; Bercaw, J. E. *J. Am. Chem. Soc.* **1994**, *116*, 4623.

Scheme 2

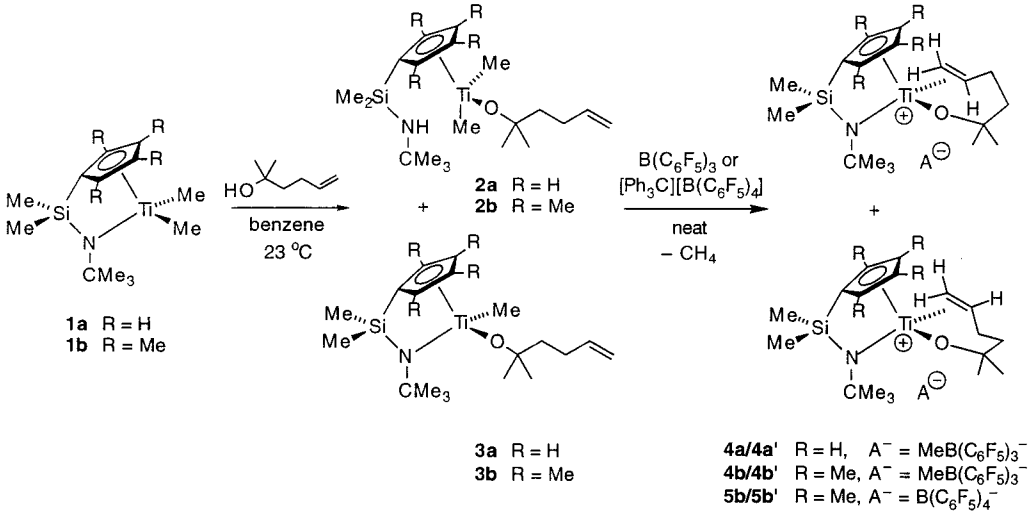

sterically open, is more electronically unsaturated, and has harder character than a 14-electron $(C_5R_5)_2ZrX^+$ species. The objectives of this work were to generate cationic species of type **IX**, determine if they adopt chelated structures, and compare the metal−olefin bonding and dynamic properties to those of zirconocene systems **I** and **II**.

Results

Neutral Ti(OCMe$_2$CH$_2$CH$_2$CH=CH$_2$) Complexes. As shown in Scheme 2, the reaction of {η^5: η^1-$C_5R_4SiMe_2N^tBu$}$TiMe_2$ (**1a**,**b**; R = H, Me) with 1 equiv of 2-methyl-5-hexene-2-ol in benzene (23 °C, 5 min) proceeds by competitive Ti−N and Ti−C bond alcoholysis to yield the monocyclopentadienyl alkoxide complexes **2a**,**b** as the major products (94 and 89% NMR yield, respectively, versus an internal standard) and the *ansa*-cyclopentadienyl-amido alkoxide complexes **3a**,**b** as the only other NMR-observable organometallic products (6 and 11% vs. internal standard, respectively).[13l,m] The ^{1}H NMR spectra of **2a**,**b** contain NH resonances (δ 0.76, 0.57; CD_2Cl_2) that are close to those for the corresponding free amines $(C_5R_4H)SiMe_2NH^tBu$.[14] Additionally, the ^{t}Bu resonances for **2a**,**b** (δ 1.09, 1.09; C_6D_6) are shifted upfield compared to the corresponding resonances for **1a**,**b** (δ 1.52, 1.57) and are close to the free amine resonances. A similar trend is observed for the -*C*Me$_3$ ^{13}C NMR resonances of **2a**,**b** which are shifted ∼10 ppm upfield from those of **1a**,**b**. In contrast, the ^{t}Bu NMR resonances for **3a**,**b** are similar to those of **1a**,**b**. The ^{1}H and ^{13}C NMR spectra of **3a** contain two Si−*Me* and four C_5H_4 resonances, and the spectra of **3b** contain two Si−*Me* and four C_5Me_4 resonances, consistent with C_1-symmetric structures.

The **2a**/**3a** and **2b**/**3b** product ratios are not affected by the presence of excess 2-methyl-5-hexene-2-ol. Mixtures of **2a**/**3a** and **2b**/**3b** were obtained as yellow-brown oils after evaporation of the solvent. These compounds are highly soluble in hexane (even at −78 °C), benzene, and chlorinated solvents and could not be separated by crystallization. The mixtures were used directly for generation of cationic species.

{η^5: η^1-$C_5R_4SiMe_2N^tBu$}Ti(OCMe$_2$CH$_2$CH$_2$CH=CH$_2$)$^+$ Species. Direct addition of solid $B(C_6F_5)_3$ to neat **2a**/**3a** and **2b**/**3b** mixtures, followed by addition of C_6D_6 by vacuum transfer, affords chelated olefin complexes **4a**/**4a′** and **4b**/**4b′** in 71 and 89% NMR yield, respectively, vs. an internal standard (Scheme 2).[15] The reaction of the **2b**/**3b** mixture with $[Ph_3C][B(C_6F_5)_4]$ under similar conditions generates the corresponding $B(C_6F_5)_4^-$ salt **5b**/**5b′** in 88% NMR yield along with Ph_3CCH_3.[15] The formation of the chelated olefin complexes from **2a**,**b** proceeds by methyl abstraction by $B(C_6F_5)_3$ or Ph_3C^+ and subsequent Ti−Me protonolysis by the NH group, which eliminates CH_4 (detected by ^{1}H NMR, δ 0.2). Compounds **4a**/**4a′**, **4b**/**4b′** and **5b**/**5b′** separate as oils from aromatic and aliphatic hydrocarbon solvents. Washing the oils with hexane and drying under high vacuum yields **4a**/**4a′**, **4b**/**4b′** and **5b**/**5b′** in 70−90% purity as red-orange gummy solids. The isolated materials are readily soluble in dichloromethane and 1,2-dichloroethane. These solutions are quite stable and can be stored for several weeks at −30 °C without noticeable reaction. However, attempts to further purify **4a**/**4a′**, **4b**/**4b′**, or **5b**/**5b′** were unsuccessful.

The structures of the cations of **4a**/**4a′**, **4b**/**4b′**, and **5b**/**5b′** in CD_2Cl_2 solution were established by NMR studies. The low-temperature (−60 °C) ^{1}H and ^{13}C NMR spectra of these species each contain two complete sets of resonances and establish that

(13) (a) Chen, Y.-X.; Marks, T. J. *Organometallics* **1997**, *16*, 3649. (b) Soga, K.; Uozomi, T.; Nakamura, S.; Toneri, T.; Teranishi, T.; Sano, T.; Arai, T. *Macromol. Chem. Phys.* **1996**, *197*, 4237. (c) Sernetz, F. G.; Mülhaupt, R.; Waymouth, R. M. *Macromol. Chem. Phys.* **1996**, *197*, 1071. (d) Shiomura, T.; Asanuma, T.; Inoue, N. *Macromol. Rapid Commun.* **1996**, *17*, 9. (e) Eberle, T.; Spaniol, T. P.; Okuda, J. *Eur. J. Inorg. Chem.* **1998**, 237. (f) Sernetz, F. G.; Mülhaupt, R.; Amor, F.; Eberle, T.; Okuda, J. *J. Polym. Sci., Part A: Polym. Chem.* **1997**, *35*, 1571. (g) Sinnema, P.-J.; Liekelema, K.; Staal, O. K. B.; Hessen, B.; Teuben, J. H. *J. Mol. Catal. A: Chem.* **1998**, *128*, 143. (h) McKnight, A. L.; Masood, M. A.; Waymouth, R. M. *Organometallics* **1997**, *16*, 2879. (i) McKnight, A. L.; Waymouth, R. M. *Chem. Rev.* **1998**, *98*, 2578. (j) Shaffer, T. D.; Canich, J. A. M.; Squire, K. R. *Macromolecules* **1998**, *31*, 5145. (k) Hultzsch, K. C.; Voth, P.; Beckerle, K.; Spaniol, T. P.; Okuda, J. *Organometallics* **2000**, 19, 228. (l) For other reactions in which the $\{C_5R_4SiMe_2N^tBu\}M$ chelate ring in constrained geometry complexes is cleaved, see: Carpenetti, D. W.; Kloppenburg, L.; Kupec, J. T.; Petersen, J. L. *Organometallics* **1996**, *15*, 1572 and (m) Kloppenburg, L.; Petersen, J. L. *Organometallics* **1996**, *15*, 7.

(14) $(C_5H_5)SiMe_2NH^tBu$ (5-isomer): ^{1}H NMR (C_6D_6) δ 6.58 (br, 2H, C_5H_4), 6.52 (br, 2H, C_5H_4), 3.50 (br s, 1H, C_5H_4H), 1.20 (s, 9H, ^{t}Bu), 0.62 (br s, ^{1}H, N*H*), −0.03 (s, 6H, SiCH_3). $(C_5Me_4H)SiMe_2NH^tBu$ (5-isomer): ^{1}H NMR (C_6D_6) δ 2.75 (br s, 1H, C_5Me_4H), 2.00 (s, 6H, C_5CH_3), 1.84 (s, 6H, C_5CH_3), 1.10 (s, 9H, ^{t}Bu), 0.39 (br s, 1H, N*H*), 0.10 (s, 6H, SiCH_3).

(15) Extensive NMR experiments utilizing an internal standard showed that **4b**/**4b′** and **5b**/**5b′** are formed in 89% yield along with 11% of a ∼1/1 mixture of two diamagnetic cationic Ti compounds with free vinyl groups. These species could not be unambiguously identified by NMR or attempted derivatization/trapping experiments. However variable temperature 1D- and 2D-EXSY ^{1}H NMR experiments established that the unidentified species do not influence the dynamic properties of **4b**/**4b′** and **5b**/**5b′** and that the free vinyl groups of the unidentified species do not exchange with those of **4b**/**4b′** and **5b**/**5b′**.

the diastereomer ratios **4a**/**4a′** and **4b**/**4b′** are 62/38 and 75/25, respectively. The diastereomer ratio of the $B(C_6F_5)_4^-$ salt **5b**/**5b′** is the same as that for the corresponding $MeB(C_6F_5)_3^-$ salt **4b**/**4b′** as expected.

The NMR data for **4a**/**4a′**, **4b**/**4b′**, and **5b**/**5b′** show that in each case the pendant olefin is coordinated to Ti. The vinyl ^{1}H resonances for each species were assigned by analysis of the J_{H-H} coupling constants and confirmed by low-temperature COSY experiments. The vinyl ^{1}H resonances are shifted substantially from the free olefin positions; in particular, the H_{int} resonance appears at low field (δ **4a**: 7.02; **4a′**: 7.24; **4b**: 6.52; **4b′**: 7.30) compared to the corresponding free olefin resonance in **2a**,**b** (δ 5.90).[16] The terminal vinyl ^{13}C resonances are shifted significantly upfield (δ C_{term} **4a**: 104.3; **4a′**: 98.0; **4b**: 106.0; **4b′**: 101.6) while the internal vinyl ^{13}C resonances are shifted significantly downfield (δ C_{int} **4a**: 159.4; **4a′**: 163.1; **4b**: 162.8; **4b′**: 167.8) from the corresponding free olefin resonances in **2a**,**b** (δ C_{term} 114.5; C_{int} 139.2). However, the vinyl J_{C-H} values for **4a**/**4a′** and **4b**/**4b′** are nearly identical to those for the free olefin, **2a**,**b** and **3a**,**b** ($J_{C-H} = 154 \pm 4$ Hz) which shows that coordination of the olefin to Ti does not significantly perturb the hybridization of the vinyl carbons. The −60 °C ^{1}H NMR spectrum of **4b**/**4b′** contains two Si−*Me* signals and four C_5Me_4 signals for each diastereomer in the expected intensity ratios, consistent with C_1-symmetric structures. Similarly, the −60 °C ^{1}H NMR spectrum of **4a**/**4a′** contains two Si−*Me* and four C_5H_4 resonances for each diastereomer.

The ^{1}H, ^{13}C, and ^{19}F NMR parameters for the $MeB(C_6F_5)_3^-$ anion in **4a**/**4a′** and **4b**/**4b′** are characteristic of the free anion.[17] The ^{1}H and ^{13}C NMR spectra of the $B(C_6F_5)_4^-$ salt **5b**/**5b′** are identical to the spectra of **4b**/**4b′** except for the anion resonances. The ^{19}F NMR spectrum of **5b**/**5b′** confirms the presence of a free $B(C_6F_5)_4^-$ anion.[18]

Addition of THF to CD_2Cl_2 solutions of **4a**/**4a′** and **5b**/**5b′** results in the formation of the THF complexes [{η^5: η^1-$C_5H_4SiMe_2N^tBu$}Ti($OCMe_2CH_2CH_2CH{=}CH_2$)(THF)][$MeB(C_6F_5)_3$] (**6a**) and [{η^5: η^1-$C_5Me_4SiMe_2N^tBu$}Ti($OCMe_2CH_2CH_2CH{=}CH_2$)(THF)][$B(C_6F_5)_4$] (**6b**). In both cases the vinyl ^{1}H and ^{13}C NMR resonances shift back to the free olefin positions, but the anion resonances are unchanged. These results confirm that the pendant olefin and not the counterion is coordinated to Ti in **4a**/**4a′** and **5b**/**5b′**.

The diastereomeric cations of **4a**/**4a′**, **4b**/**4b′**, and **5b**/**5b′** differ in the enantioface of the olefin that is coordinated and therefore in the relative configurations of the Ti center and the internal vinyl carbon (Figure 1). The structures of **4b** and **4b′** were assigned from a low-temperature (−40 °C) ^{1}H 2D NOESY spectrum. For this purpose, models of **4b** and **4b′** were generated by molecular modeling (see Experimental Section). The stereochemistry of these species is denoted by the descriptors *R*,*S* (*ent* = *S*,*R*) and *S*,*S* (*ent* = *R*,*R*), in which first entry denotes the configuration at Ti and the second entry denotes that at C_{int}.

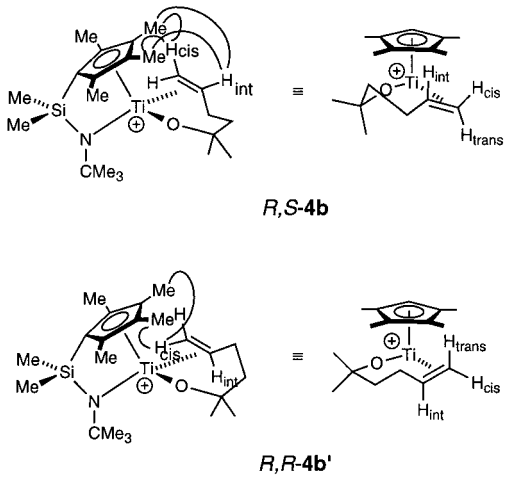

Figure 1. Side views (left) and front views (right) of *R*,*S*-**4b** and *R*,*R*-**4b′**. The curved lines in the side views show observed NOE correlations. The $SiMe_2N^tBu$ unit has been omitted for clarity in the front views.

As illustrated in Figure 1, H_{cis} and H_{int} of the major diastereomer **4b** show NOE correlations to C_5Me_4 hydrogens (δ 2.18 and 2.22), while only H_{cis} (but not H_{int}) of the minor diastereomer **4b′** correlates with a C_5Me_4 group (δ 2.24). Analysis of the models shows that these correlations are consistent with the *R*,*S* (*ent* = *S*,*R*) configuration for **4b** and the *S*,*S* (*ent* = *R*,*R*) configuration for **4b′**.[19]

Dynamic Properties of 4b/4b′. Compound **4b**/**4b′** was selected for detailed dynamic NMR studies because this species is obtained in higher purity than **4a**/**4a′** and the vinyl and Si−*Me* regions of the ^{1}H NMR spectra are relatively simple. To simplify the nomenclature in the following discussion, the diastereomers **4b** and **4b′** will be denoted as **A** and **B** respectively. As shown in Figure 2, the pairs of H_{int}, H_{trans}, and H_{cis} ^{1}H NMR resonances each collapse to a single resonance as the temperature is raised from −60 to 60 °C. The **A**/**B** (i.e., **4b**/**4b′**) ratio is constant from −60 to 20 °C (75/25 ± 2%), and the coalesced vinyl resonances at 60 °C appear at the weighted averages of the individual low-temperature (−60 °C) chemical shifts.[20] These observations establish that the **A**/**B** ratio does not change significantly between −60 and 60 °C. Additionally, as shown in Figure 3, the four Si−*Me* resonances (two for each diastereomer) broaden, coalesce, and sharpen to one singlet between −60 and 60 °C. The eight C_5Me_4 resonances (four α, four β; vs. $SiMe_2N^tBu$ bridge) also broaden and coalesce to two singlets (α, β) over this temperature range. These line-shape changes are all reversible upon lowering the temperature.

These observations imply that **4b**/**4b′** undergo two exchange processes which are illustrated in Scheme 3: (a) interconversion of **4b**/**4b′**, that is, "olefin face exchange", which permutes the corresponding vinyl hydrogens, Si−*Me* and C_5Me_4 groups of the two diastereomers (horizontal process in Scheme 3), and (b) inversion of configuration at Ti, which permutes the two Si−*Me* groups, the two α-C_5Me_4 groups and the two β-C_5Me_4 groups of each diastereomer. This second process presumably involves migration of the η^1-alkoxide ligand between lateral sites on Ti (i.e., "O-shift", vertical process in Scheme 3) in the olefin-

(16) H_{trans} and H_{cis} are *trans* and *cis* to H_{int}, respectively.

(17) The $MeB(C_6F_5)_3^-$ NMR resonances of **4a**/**4a′**, **4b**/**4b′** and **6a** are nearly identical to those of [NBu_3CH_2Ph][$MeB(C_6F_5)_3$] (see ref 3a): ^{1}H NMR (CD_2Cl_2, −60 °C) δ 0.33; (−20 °C) δ 0.41; (20 °C) δ 0.47 (br s, 3H, BCH_3). ^{13}C NMR (CD_2Cl_2, −60 °C) δ 147.3 (dm, $J_{C-F} \sim 238$), 136.8 (dm, $J_{C-F} \approx 240$, C_{para}), 135.7 (dm, $J_{C-F} \approx 243$), 127.2 (br s, C_{ipso}), 9.1 (br q, $J_{C-H} = 119$, CH_3B). ^{19}F NMR (CD_2Cl_2) δ −131.7 (d, $^3J_{F-F} = 19.9$, 2F, *o*-F), −163.5 (t, $^3J_{F-F} = 19.8$, 1F, *p*-F), −166.1 (t, $^3J_{F-F} = 19$, 2F, *m*−F). ^{11}B NMR (CD_2Cl_2) δ −13.3.

(18) $B(C_6F_5)_4^-$ resonances of **5b**/**5b′**: ^{13}C NMR (CD_2Cl_2, −60 °C) δ 146.0 (dm, $J_{C-F} \approx 238$), 137.1 (dm, $J_{C-F} \approx 240$, C_{para}), 135.4 (dm, $J_{C-F} \approx 243$), 122.9 (br s, C_{ipso}). ^{19}F NMR (CD_2Cl_2) δ −132.8 (d, $^3J_{F-F} = 21$, 8F, *o*-F), −163.5 (t, $^3J_{F-F} = 20$, 4F, *p*-F), −167.4 (br t, $^3J_{F-F} = 19$, 8F, *m*−F). ^{11}B NMR (CD_2Cl_2) δ −13.5.

(19) H−H contacts estimated by molecular modeling are as follows. **4b**: $H_{int}-C_5Me_4 = 2.7$ Å; $H_{cis}-C_5Me_4 = 2.4$ Å; **4b′**: $H_{int}-C_5Me_4 > 4.8$ Å; $H_{cis}-C_5Me_4 = 2.4$ Å. NOE correlations between H_{trans} and the C_5Me_4 groups were not observed for either diastereomer, despite the close contact ($H_{trans}-C_5Me_4 = 2.5$ Å) predicted for the *R*,*R* isomer. Close $H_{trans}-C_5Me_4$ contacts are not present in the *S*,*R* isomer ($H_{trans}-C_5Me_4 = 3.9$ Å).

(20) The chemical shifts ($\delta_{observed}$, $\delta_{calculated}$) for the vinyl hydrogen resonances at coalescence are as follows: H_{int}: 6.75, 6.76; H_{trans}: 4.90, 4.92; H_{cis}: 4.39, 4.37.

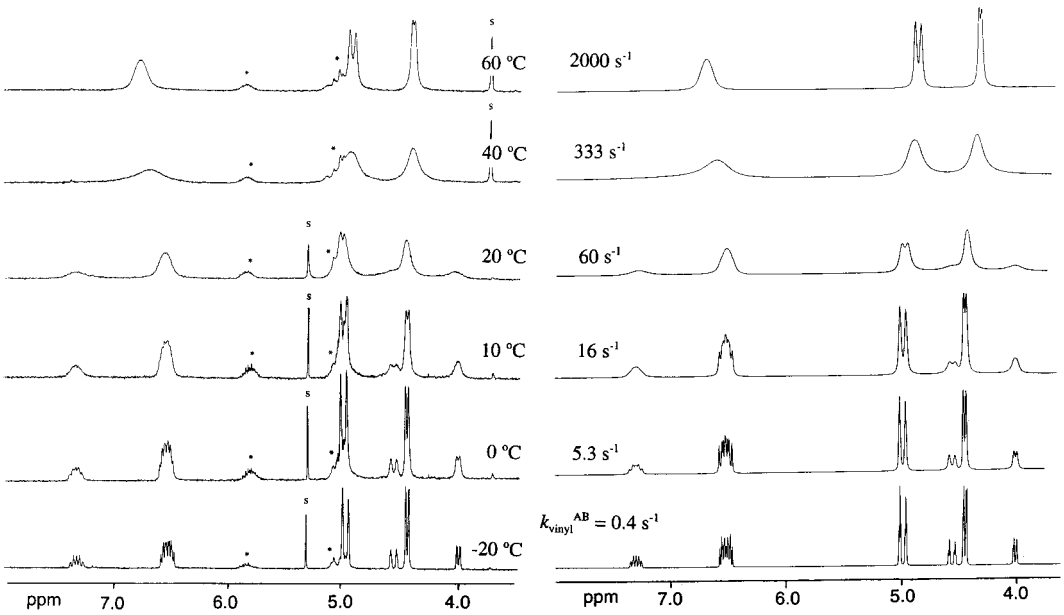

Figure 2. Experimental (left) and simulated (right) ^{1}H NMR spectra (vinyl region) of [{η^5: η^1-$C_5Me_4SiMe_2N^tBu$}Ti($OCMe_2CH_2CH_2CH{=}CH_2$)][$MeB(C_6F_5)_3$] (**4b**/**4b′** = **A**/**B**). Best-fit first-order rate constants (k_{vinyl}^{AB}) are shown with the simulated spectra. The spectra at −20 °C and −60 °C (not shown) are nearly identical. Assignments (**4b**/**4b′**): H_{int}: 6.52/7.30; H_{trans}: 4.99/4.56; H_{cis}: 4.45/4.01. * = impurities (see ref 15). S = solvent (−20 to 20 °C: CD_2Cl_2; 40 and 60 °C: CD_2ClCD_2Cl).

Scheme 3

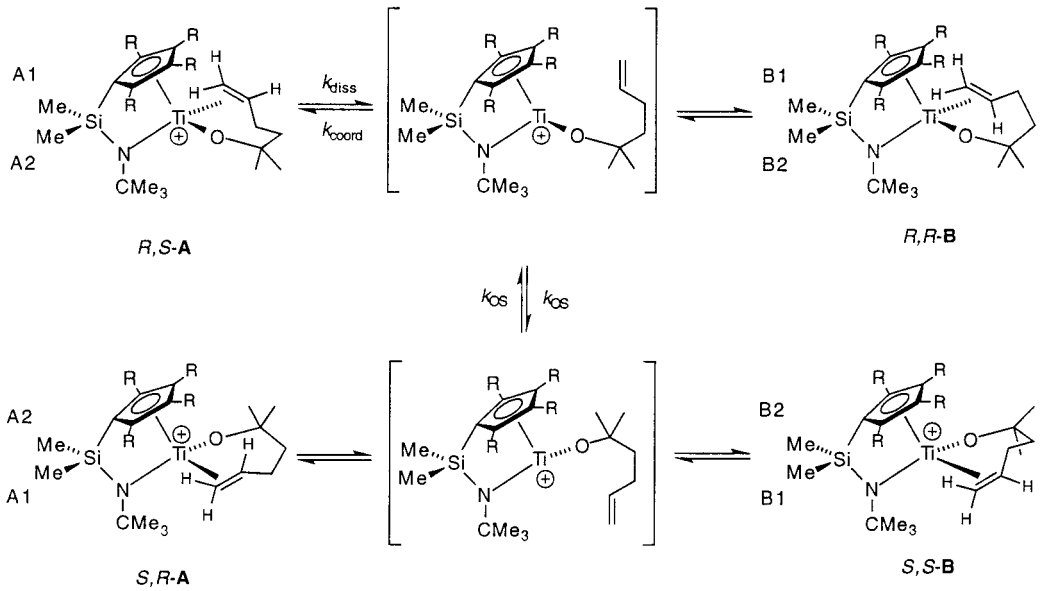

dissociated intermediate. The O-shift cannot occur if the olefin remains coordinated.[21]

Olefin Face Exchange of 4b/4b′. The kinetics of the olefin face-exchange process (i.e., **A**/**B** interconversion) were probed by line-shape analysis of the vinyl region of the ^{1}H NMR spectra (−20 to 60 °C, Figure 2). Spectra were simulated for an ensemble of three two-site exchange systems, each with a 75/25 relative population ratio, corresponding to H_{int}^A/H_{int}^B, H_{trans}^A/H_{trans}^B, and H_{cis}^A/H_{cis}^B. Satisfactory agreement between the observed and simulated spectra was only obtained when the exchange rate for each two-site system was equal, which confirms that the vinyl group undergoes face exchange as a unit. The activation parameters for the conversion of the major diastereomer (**A**) to the minor diastereomer (**B**) ($\Delta H^{\ddagger}_{vinyl}{}^{AB}$ = 17.2(8) kcal/mol; $\Delta S^{\ddagger}_{vinyl}{}^{AB}$ = 8(1) eu) were obtained from a least-squares Eyring analysis (Figure 4) according to eq 1, where k_{vinyl}^{AB} is the corresponding first-order rate constant and k_B is the Boltzmann constant.

$$\ln(k_{vinyl}{}^{AB}/T) = -\Delta H^{\ddagger}_{vinyl}{}^{AB}/(RT) + (\Delta S^{\ddagger}_{vinyl}{}^{AB}/R) + \ln(k_B/h) \quad (1)$$

The face-exchange process was also investigated in the slow-exchange region (−40 to 0 °C) by two-dimensional exchange spectroscopy. Representative phase-sensitive ^{1}H 2D NOESY-EXSY spectra (vinyl region) of **A**/**B** (**4b**/**4b′**) in CD_2Cl_2 are shown in Figure 5. At −40 °C a nearly pure NOESY spectrum is obtained, as cross-peaks arise almost exclusively between signals of the same diastereomer. Additionally however, low-

(21) Four TiOC*Me*$_2$− signals are observed at −60 °C for **4b**/**4b′** (two for each diastereomer). These signals coalesce to one singlet at 60 °C, which is consistent with the existence of the two exchange processes noted in the text.

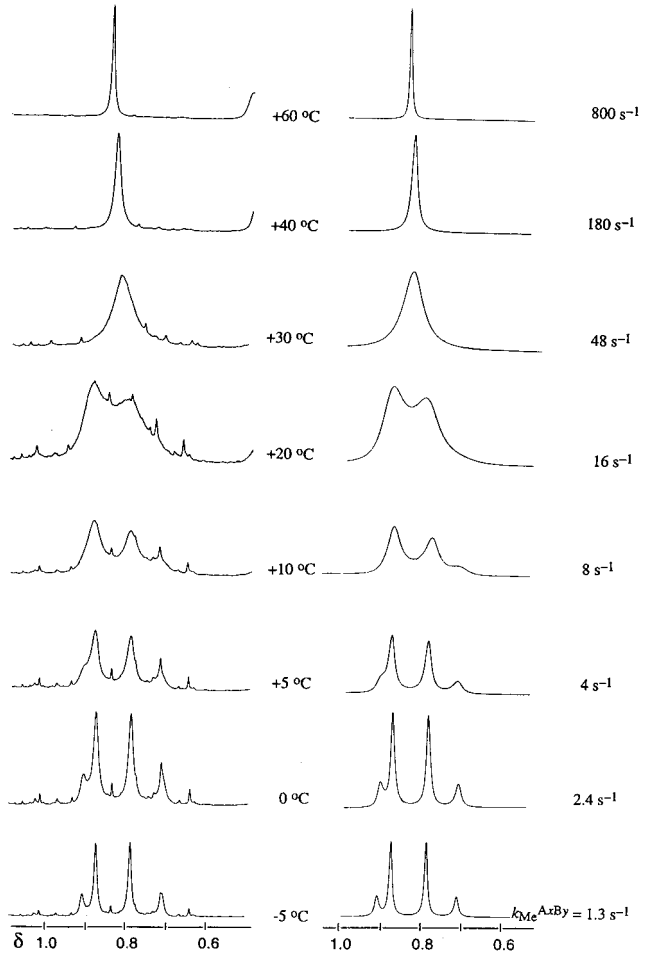

Figure 3. Experimental (left) and simulated (right) ^{1}H NMR spectra (Si−*Me* region) of [{η^5: η^1-$C_5Me_4SiMe_2N^tBu$}Ti($OCMe_2CH_2CH_2CH{=}CH_2$)][MeB(C_6F_5)$_3$] (**4b**/**4b′** = **A**/**B**). Best-fit first-order rate constants (k_{Me}^{AxBy}) are shown with the simulated spectra. Assignments: **4b**: δ 0.87, 0.79; **4b′**: δ 0.91, 0.71.

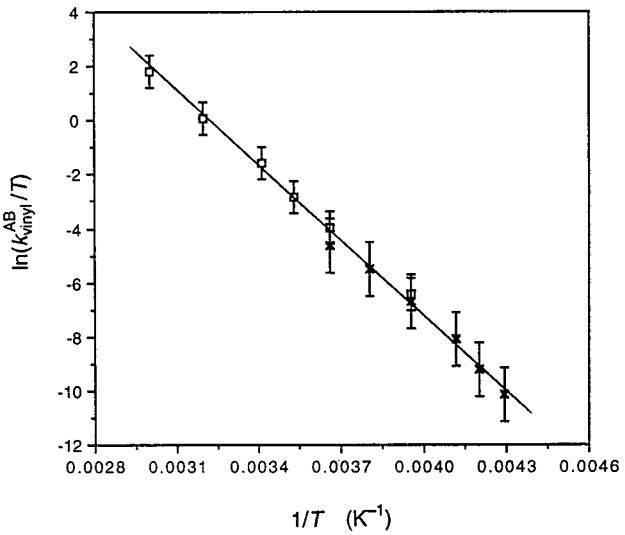

Figure 4. Eyring plot of "olefin face-exchange" rate constants (k_{vinyl}^{AB}) for [{η^5: η^1-$C_5Me_4SiMe_2N^tBu$}Ti($OCMe_2CH_2CH_2CH{=}CH_2$)][MeB(C_6F_5)$_3$] (**4b**/**4b′** = **A**/**B**) using line-shape (□) and 2D-EXSY (×) data. The line corresponds to the overall least-squares fit.

intensity cross-peaks are detected between H_{cis}^A and H_{cis}^B, indicating that chemical exchange is not totally frozen at this temperature. As the temperature is increased, the intensities of the exchange cross-peaks increase. Between −35 and 0 °C, the

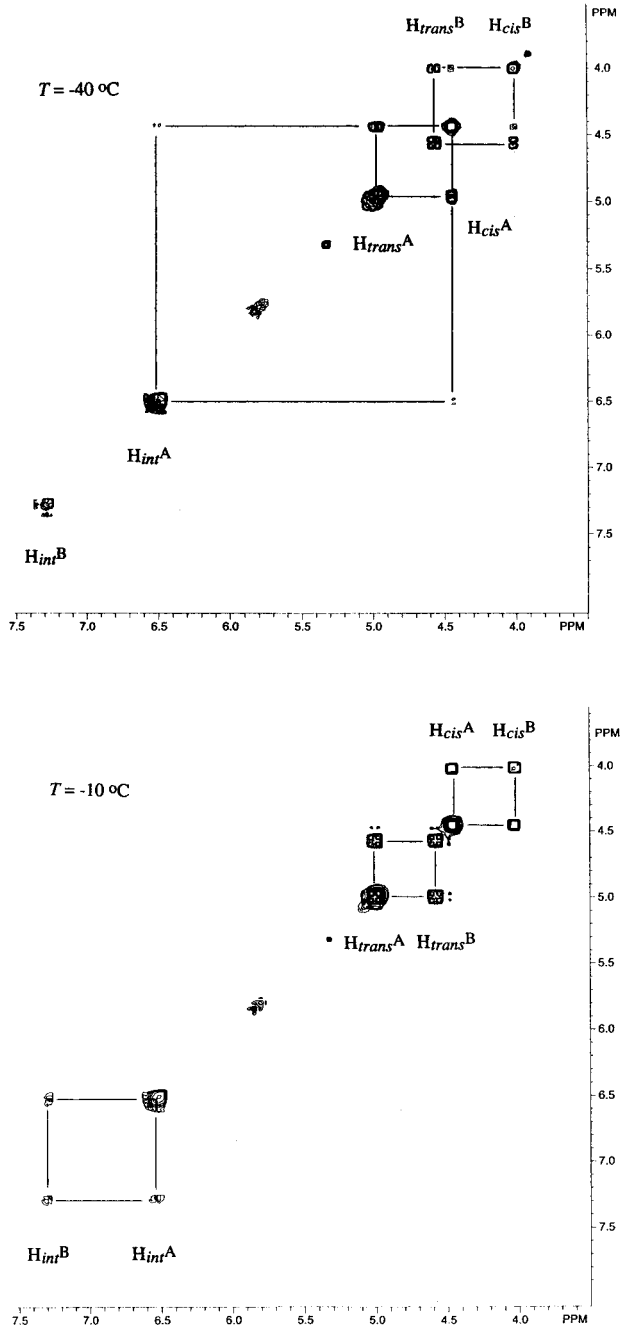

Figure 5. 360-MHz ^{1}H 2D-NOESY/EXSY spectra (vinyl region) of [{η^5: η^1-$C_5Me_4SiMe_2N^tBu$}Ti($OCMe_2CH_2CH_2CH{=}CH_2$)][MeB(C_6F_5)$_3$] (**4b**/**4b′** = **A**/**B**) in CD_2Cl_2 solution. The spectrum at −40 °C (top) shows almost exclusively NOESY correlations within **4b** and **4b′** (correlations drawn), while the spectrum at −10 °C (bottom) shows exchange between **4b** and **4b′** (exchange networks drawn).

spectra display high-intensity cross-peaks for each pair of vinyl hydrogens, H_{trans}^A/H_{trans}^B, H_{cis}^A/H_{cis}^B, and H_{int}^A/H_{int}^B, as expected for the face-exchange process.

The 2D EXSY data were treated quantitatively using the methods summarized by Perrin and Dwyer.[22] Each of the three sets of diagonal and cross-peak intensities were processed, assuming a two-site exchange system according to eqs 2 and 3, in which k' is the sum of forward and reverse exchange rate constants in s^{-1}, τ_m is the mixing time, X denotes the mole

(22) (a) Perrin, C. L.; Dwyer, T. J. *Chem. Rev.* **1990**, *90*, 935. See also: (b) Orrell, K. G.; Sik, V. Dynamic NMR Spectroscopy in Inorganic and Organometallic Chemistry. In *Annual Reports in NMR Spectroscopy*; Webb, G. A., Ed.; Academic: New York, 1993; Vol. 27, pp 103−172.

Scheme 4

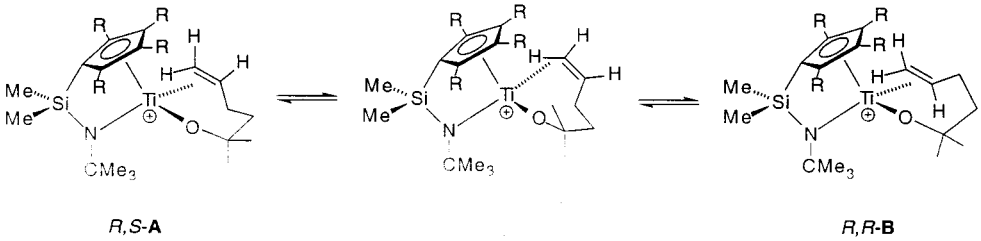

R,S-**A** *R,R*-**B**

Table 1. Olefin Face-Exchange Rate Constants Derived from the ^{1}H EXSY Spectra of **4b**/**4b′**[a]

T, °C	τ_m, s	k' (H_{trans}), s^{-1}	k' (H_{cis}), s^{-1}	k_{vinyl}^{AB}, s^{-1} [b]
−40	1.0	0.02(2)	0.05(2)	0.009(5)
−35	0.5	0.08(2)	0.11(2)	0.024(5)
−30	0.4	0.29(4)	0.32(3)	0.076(9)
−20	0.3	1.23(7)	1.35(8)	0.32(2)
−10	0.2	4.5(3)	4.3(3)	1.10(8)
0	0.05	10(1)	10(1)	2.6(2)

[a] See Experimental Section. [b] Rate constant calculated from $k'_{average} = [k'(H_{trans}) + k'(H_{cis})]/2$ according to eq 5.

fractions of the two sites ($X_A = 0.75$; $X_B = 0.25$), I_{AA} and I_{BB} are the diagonal peak intensities, and I_{AB} and I_{BA} are the cross-peak intensities.

$$k' = (1/\tau_m) \times \ln[(r+1)/(r-1)] \quad (2)$$

$$r = \{4X_AX_B(I_{AA} + I_{BB})/(I_{AB} + I_{BA})\} - (X_A - X_B)^2 \quad (3)$$

Considering that the forward and reverse rates (R^{AB}, R^{BA}) are equal (eq 4), the rate constant for conversion of **A** to **B** (k_{vinyl}^{AB}) is given by eq 5:

$$R^{AB} = X_A k_{vinyl}^{AB} = X_B k_{vinyl}^{BA} = R^{BA} \quad (4)$$

$$k_{vinyl}^{AB} = k'/(1 + X_A/X_B) \quad (5)$$

The k' values determined by analysis of the H_{trans} and H_{cis} signals between −40 and 0 °C are listed in Table 1 and agree within experimental error, as expected for an exchange process in which the whole vinyl unit is involved.[23] For each temperature, the $k'(H_{trans})$ and $k'(H_{cis})$ values were averaged and used to determine k_{vinyl}^{AB}. Activation parameters for the face-exchange process ($\Delta H^{\ddagger}_{vinyl}{}^{AB} = 17.5(8)$ kcal/mol; $\Delta S^{\ddagger}_{vinyl}{}^{AB} = 8(2)$ eu) were obtained by an Eyring analysis of these k_{vinyl}^{AB} values (Figure 4). These values agree well with the values determined by the line-shape analysis described above.

Possible Olefin Face-Exchange Mechanisms. The most likely mechanism for the olefin face exchange is a simple olefin dissociation/recoordination process (Scheme 3). Associative mechanisms involving displacement of the olefin by the anion can be ruled out because the ^{1}H NMR spectra of the $MeB(C_6F_5)_3^-$ salt **4b**/**4b′** and $B(C_6F_5)_4^-$ salt **5b**/**5b′** are identical in the range −60−70 °C (except for the anion resonances).[24] It is more difficult to probe the extent to which olefin dissociation is assisted by the solvent, due to the solubility and reactivity properties of these compounds. The ^{1}H NMR spectra of **4b**/**4b′** in CD_2Cl_2 are identical to those in $ClCD_2CD_2Cl$ over the range 10 to 30 °C (intermediate exchange region), but the polarity and donor properties of these solvents are very similar. **4b**/**4b′** is not stable in C_6D_5Cl. The positive $\Delta S^{\ddagger}$ value (8(1) eu) is consistent with simple olefin dissociation with minimal solvent involvement, although this value should be interpreted with caution.[25]

An alternative possible face-exchange mechanism is a non-dissociative mechanism involving transit of the Ti center through the alkene π nodal plane via a C−H σ-complex without complete olefin dissociation, as illustrated in Scheme 4. Mechanisms of this type have been proposed previously for the interconversion of diastereomeric Re−olefin complexes.[26] Analysis of the vinyl region of the ^{1}H NMR spectra of **4b**/**4b′** does not allow the dissociative and σ-complex mechanisms to be distinguished. However, this issue can be addressed by analysis of the Si−*Me* exchange, as described in the next section.

Si−Me Exchange. The Si−*Me* exchange system comprises four sites which are labeled A1, A2, B1, and B2 in Scheme 3. A1 and A2 correspond to the diastereotopic Si−*Me* groups of the major diastereomer **A** (**4b**), and B1 and B2 correspond to the diastereotopic Si−*Me* groups of the minor diastereomer **B** (**4b′**). Interconversion of *R,S*-**A** and *S,R*-**A** permutes A1 and A2, while interconversion of *R,R*-**B** and *S,S*-**B** permutes B1 and B2. Because the diastereomer ratio **A**/**B** = 3/1, the relative populations (mole fractions) of sites A1, A2, B1, and B2 are 3/8, 3/8, 1/8, and 1/8, respectively.

Assuming that (i) olefin face exchange (i.e., **A**/**B** interconversion) occurs by olefin dissociation/recoordination and (ii) the O-shift is much faster than olefin recoordination in the olefin-dissociated intermediate, that is, $k_{OS} \gg k_{coord}$ in Scheme 3, then exchange of the Si−*Me* groups should proceed statistically, according to the relative populations of the different sites. The existence of four Si−*Me* sites implies six possible site-to-site exchanges (A1−A2, A1−B1, A1−B2, A2−B1, A2−B2, B1−B2). The rate of each site-to-site exchange R_{ij} is given by eq 6

$$R_{ij} = p_{ij} \times P_i \times k \quad (6)$$

where p_{ij} is the probability of exchanging from site i to j, P_i is the population of site i, and k is defined in terms of the mean lifetime τ of all sites by $k = 1/\tau$.[22,27] Also, equilibrium mass

(23) Accurate kinetic data could not be extracted from the H_{int} signals due to the high multiplicity and the significant broadening of these signals with increasing temperature, which precluded determination of accurate cross−peak volume intensities.

(24) Variable temperature ^{1}H NMR spectra were recorded for **4b**/**4b′** over a 2−fold concentration range, and no concentration dependence was noted.

(25) Purely associative mechanisms are generally characterized by $\Delta S^{\ddagger}$ values below −10 eu. However, activation entropies are difficult to determine precisely and must be interpreted carefully because of possible contributions from solvent reorganization, especially for polar solvents and charged metal complexes; see: (a) Atwood, J. D. *Inorganic and Organometallic Reaction Mechanisms*; Brooks/Cole: Monterey, CA, 1985; p 17. (b) Jordan, R. B. *Reaction Mechanisms of Inorganic and Organometallic Systems*; Oxford University: New York, 1991; pp 56−57.

(26) (a) Peng, T.-S.; Gladysz, J. A. *J. Am. Chem. Soc.* **1992**, *114*, 4174. See also: (b) Kegley, S. E.; Walter, K. A.; Bergstrom, D. T.; MacFarland, D. K.; Young, B. G.; Rheingold, A. L. *Organometallics* **1993**, *12*, 2339. (c) Quirós-Méndez, N.; Mayne, C. L.; Gladysz, J. A. *Angew. Chem., Int. Ed. Engl.* **1990**, *29*, 1475.

(27) For a discussion of the relationship between rate constants measured by dynamic NMR methods and those of the chemical process(es) giving rise to the exchange, see: Green, M. L. H.; Wong, L. L.; Sella, A. *Organometallics* **1992**, *11*, 2660.

balance requires that

$$R_{ij} = R_{ji} = p_{ji} \times P_j \times k \quad (7)$$

Thus, the rate of exchange of A1 and A2, which corresponds to interconversion of the two enantiomers of the major diastereomer **A**, is expected to be 9 times faster ($R_{A1A2} = 3/8 \times 3/8 \times k$) than the rate of exchange of B1 and B2, which corresponds to the interconversion of the two enantiomers of the minor diastereomer **B** ($R_{B1B2} = 1/8 \times 1/8 \times k$). The four "cross-exchanges", that is, A1−B1, A1−B2, A2−B1, and A2−B2 (A*x*−B*y*; *x*,*y* = 1 or 2), which correspond to interconversion of the major and minor diastereomers, occur at an intermediate rate ($R_{AxBy} = 3/8 \times 1/8 \times k$). Thus, if assumptions (i) and (ii) are correct, it is expected that the six possible site-to-site exchanges A1−A2, A1−B1, A1−B2, A2−B1, A2−B2, B1−B2 should occur at relative rates of 9/3/3/3/3/1.

On the other hand, if the O-shift is not fast relative to olefin recoordination (i.e., $k_{OS} \leq k_{coord}$ in Scheme 2), then the four Si−*Me* exchanges that require olefin dissociation *and* O-shift, that is, A1−A2, A1−B2, A2−B1, and B1−B2, would occur at slower rates than the A1−B1 and A2−B2 exchanges. This result would also be observed if a nondissociative pathway such as the "*σ*-complex" mechanism (Scheme 4) contributes significantly to the face-exchange process.

The Si−*Me* region was simulated assuming that the six possible exchanges of the four Si−*Me* sites (A1−A2, A1−B1, A1−B2, A2-B1, A2−B2, B1−B2) occur at relative rates of 9/3/3/3/3/1. The site-to-site exchange rates were optimized to fit the simulated and experimental spectra of **4b**/**4b′** over the temperature range −5 to 60 °C, which includes the intermediate and fast exchange regions. As shown in Figure 3, a good fit was obtained using this procedure. Exhaustive simulations showed that for the spectrum at 10 °C (intermediate exchange region), which proved to be very sensitive to the simulation parameters, a satisfactory match of observed and simulated spectra requires that the relative A1−A2, A1−B1, A1−B2, A2−B1, A2−B2, and B1−B2 exchange rates be close to 9/3/3/3/3/1.[28] On the basis of these results, we conclude that *σ*-complex intermediates do not play a significant role in the face exchange of **4b**/**4b′**. The rate constants for the "cross-exchanges" ($k_{Me}^{AxBy} = k_{Me}^{A1B1} = k_{Me}^{A1B2} = k_{Me}^{A2B1} = k_{Me}^{A2B2}$) obtained by this procedure are given in Figure 3.[29]

At this stage it is useful to relate the rate constants for (a) the Si−*Me* site-to-site exchanges (k_{Me}^{AxBy}), (b) the olefin face exchange determined from analysis of the vinyl region (k_{vinyl}^{AB}), and (c) the olefin dissociation (k_{diss}). As is evident from Scheme 3, if assumptions (i) and (ii) above are correct, then because the isomer ratio **A**/**B** = 3/1, the exchange of a given Si−*Me* of **A** with a given Si−*Me* of **B** occurs in one out of eight dissociation events, that is,

$$k_{Me}^{AxBy} = k_{diss}/8 \quad (8)$$

Similarly, the exchange of each of the three vinyl hydrogens of **A** with the corresponding vinyl hydrogens of the **B** occurs in one out of four dissociation events, that is,

$$k_{vinyl}^{AB} = k_{diss}/4 \quad (9)$$

Consequently it is expected that

$$2k_{Me}^{AxBy} = k_{vinyl}^{AB} \quad (10)$$

As shown in Table 2, the values of k_{Me}^{AxBy} and k_{vinyl}^{AB} are consistent with eq 10. Accordingly, the values of $2k_{Me}^{AxBy}$ were used in an Eyring analysis (Figure 6) to calculate the activation parameters for the olefin face exchange determined by the Si−*Me* simulation ($\Delta H^{\ddagger}_{Me}{}^{AB} = 17.0(7)$ kcal/mol; $\Delta S^{\ddagger}_{Me}{}^{AB} = 7(2)$ eu). These values agree well with those determined from analysis of the vinyl region.

In summary, the following key results emerge from our study of the dynamic properties of **4b**/**4b′**: (i) the vinyl group undergoes face exchange as a unit, (ii) the dynamic properties are not influenced by the counterion, which implies that the

Table 2. Comparison of k_{Vinyl}^{AB} and k_{Me}^{AxBy} Values[a]

T, °C	k_{vinyl}^{AB}, s^{-1}	$2k_{Me}^{AxBy}$, s^{-1}
−5	2.3	2.7
0	4.4	4.8
5	8.2	8
10	16	16
20	46	32
30	133	96
40	358	360
60	2183	1600

[a] Values of k_{vinyl}^{AB} were calculated using activation parameters derived from the least-squares Eyring analysis of the combined lineshape and EXSY data (see Figure 4).

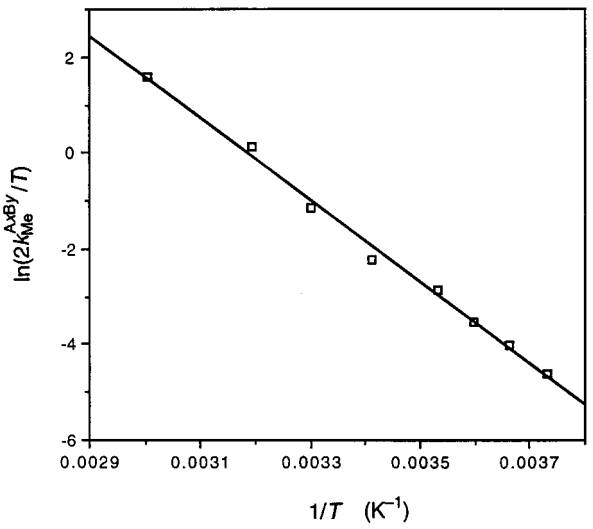

Figure 6. Eyring plot of "olefin face-exchange" rate constants ($2k_{Me}^{AxBy}$) for [{η^5: η^1-$C_5Me_4SiMe_2N^tBu$}Ti($OCMe_2CH_2CH_2CH{=}CH_2$)]-[$MeB(C_6F_5)_3$] (**4b**/**4b′**) determined from simulation of the Si−*Me* region.

(28) However, it should be pointed out that at other temperatures, the spectra are less sensitive to the simulation parameters. For example, for 0 °C, a satisfactory fit between experimental and simulated spectra can also be obtained by using relative rates for the six Si−*Me* permutations varying by up to ∼±40% from the statistical ratio 9/3/3/3/3/1.

(29) The results of the simulation were confirmed by line-broadening analysis in the slow exchange region (−5−5 °C). Under conditions of dissociative olefin face exchange and fast O−shift (Scheme 3), the rate constant for exchange of a given Si−*Me* group of **A** to *any* of the other three Si−*Me* sites in **A** or **B** (k_{Me}^{A}) is related to the site-to−site rate constants by $k_{Me}^{A} = k_{Me}^{A1A2} + k_{Me}^{A1B1} + k_{Me}^{A1B2}$. From eq 6, $k_{Me}^{A1A2} = 3k_{Me}^{AxBy}$, so that $k_{Me}^{A} = 5k_{Me}^{AxBy}$. Similarly, the rate constant for exchange of a given Si−*Me* group of **B** to any of the other three Si−*Me* sites (k_{Me}^{B}) is given by $k_{Me}^{B} = k_{Me}^{B1B2} + k_{Me}^{B1A1} + k_{Me}^{B1A2}$. From eq 6, $k_{Me}^{B1B2} = k_{Me}^{AxBy}$ and $k_{Me}^{BxAy} = 3k_{Me}^{AxBy}$, so that $k_{Me}^{B} = 7k_{Me}^{AxBy}$. Values for k_{Me}^{A} and k_{Me}^{B} were obtained from the excess line widths of the Si−*Me* resonances in the slow exchange region (−5−5 °C) using the relation $k = \pi(\Delta W)$, where $\Delta W = W - W_0$, W is the line width at half−height, and W_0 is the line width in the absence of exchange (W_0 = 1.5 Hz, measured at −40 and −60 °C). The rate constants determined by this analysis agree well with the values determined by simulation. k_{Me}^{A} (line broadening, simulation; s^{-1}): −5 °C: 6.0, 6.7; 0 °C: 11.2, 12.0; 5 °C: 20.4, 20.0. k_{Me}^{B} (line broadening, simulation): −5 °C: 8.5, 9.3; 0 °C: 16.7, 16.8).

face exchange is not assisted by the anion, and (iii) the Si−*Me* exchange is statistical, and the activation parameters for the vinyl exchanges and Si−*Me* exchange are identical within experimental uncertainty. These results are best accommodated by Scheme 3, in which the rate-limiting step is olefin dissociation and inversion of configuration at Ti in the olefin-dissociated intermediate is fast relative to olefin recoordination. Nondissociative olefin face exchange via σ-complex intermediates is not important in this system. It is possible that the solvent assists the olefin dissociation and stabilizes the olefin-dissociated intermediate, but the positive $\Delta S^{\ddagger}$ value argues against kinetically significant solvent participation.

Dynamic Properties of 4a/4a′. The dynamic properties of **4a**/**4a′** are similar to those of **4b**/**4b′** and are discussed briefly in this section. The ^{1}H NMR spectrum of **4a**/**4a′** (CD_2Cl_2) at 23 °C contains a single set of sharp resonances for the Si−*Me*, ^{t}Bu, TiOC*Me*$_2$, α-C_5H_4, and β-C_5H_4 hydrogens, indicating that interconversion of **4a** and **4a′** (olefin face exchange) and inversion of configuration at Ti (O-shift) are fast on the chemical shift time scale at this temperature. The kinetics of the **4a**/**4a′** exchange were probed by analysis of the vinyl region of the ^{1}H NMR spectrum. As the temperature is raised from −60 to 23 °C, the pairs of H_{int}, H_{trans}, and H_{cis} ^{1}H NMR resonances each collapse to a single resonance. The **4a**/**4a′** ratio is constant from −60 to 23 °C (62/38 ± 2%), and the coalesced vinyl resonances at 23 °C appear close to the weighted average of the individual low-temperature (−60 °C) chemical shifts.[30] Activation parameters for the face-exchange process ($\Delta H^{\ddagger}_{vinyl}{}^{\mathbf{4a/4a'}} = 12.2(9)$ kcal/mol; $\Delta S^{\ddagger}_{vinyl}{}^{\mathbf{4a/4a'}} = -2(3)$ eu) were determined by line-shape analysis of the H_{cis} resonances over the temperature range −40−23 °C.[31]

Discussion

Methyl abstraction from **2a**/**3a** and **2b**/**3b** mixtures yields the cationic d^0 metal olefin complexes {η^5: η^1-$C_5R_4SiMe_2N^tBu$}-Ti(OCMe_2CH_2CH_2CH=CH_2)$^+$ (R = Me in **4b**/**4b′**; R = H in **4a**/**4a′**). The NMR data for these cations are very similar to the data for **I** and **II**, for which unsymmetrical Zr−olefin bonding was established by X-ray crystallography. In particular, the H_{int} ^{1}H resonances and the C_{int} ^{13}C resonances for **4b**/**4b′** and **4a**/**4a′** are shifted significantly downfield, and the C_{term} ^{13}C resonances are shifted significantly upfield, from the free olefin positions, as observed for **I** and **II**. The olefin J_{C-H} values in **4b**/**4b′** and **4a**/**4a′** are unchanged from the free olefin values. These results are consistent with unsymmetrical Ti−olefin bonding in **4b**/**4b′** and **4a**/**4a′**; that is, the Ti−olefin bond in these systems comprises a weak Ti−C_{term} and minimal Ti−C_{int} interaction which results in polarization of the C=C π bond with positive charge buildup at C_{int}. As proposed for **I** and **II**, a σ-bonded resonance form **XII** thus contributes to the structures **4b**/**4b′** and **4a**/**4a′** (Chart 2). The NMR data for the coordinated olefin units in the chelated alkyl olefin complexes **V**, **VI**, and $Cp^*_2YCH_2CH_2CRR'CH{=}CH_2$, and the nonchelated propene complex **VIII** are also consistent with unsymmetrical M−olefin bonding. Thus, unsymmetrical metal−olefin bonding appears to be a general feature of the ground-state structures of d^0 metal

Chart 2

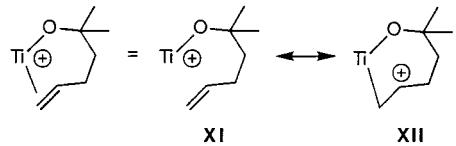

XI **XII**

Table 3. Activation Parameters for Olefin Face Exchange of $L_nM(OCMe_2CH_2CH_2CH{=}CH_2)^+$ Complexes from Dynamic ^{1}H NMR Studies

L_nM^+	$\Delta H^{\ddagger}$ kcal/mol	$\Delta S^{\ddagger}$ eu	$\Delta G^{\ddagger}$ at 298 K kcal/mol
Cp_2Zr^+ (**I**)	9.6(5)[a]	−5(2)[a]	11.1(8)[a]
rac-(EBI)Zr$^+$ (**II**)	16.2(4)[b]	3(2)[b]	15.3(7)[b]
{η^5: η^1−$C_5H_4SiMe_2N^tBu$}Ti$^+$ (**4a**/**4a′**)	12.2(9)[c]	−2(3)[c]	13(1)[c]
{η^5: η^1−$C_5Me_4SiMe_2N^tBu$}Ti$^+$ (**4b**/**4b′**)	17.2(8)[c]	8(2)*c*	15(1)[c]

[a] Determined by analysis of ZrOC*Me*$_2$ region; ref 3a. [b] Determined by analysis of Me_{syn} region; ref 3a. [c] Values for conversion of major to minor diastereomer determined by analysis of vinyl region; this work.

α-olefin complexes in both metallocene and constrained geometry systems.

The activation parameters for olefin face exchange of the $L_nM(OCMe_2CH_2CH_2CH{=}CH_2)^+$ complexes that we have investigated to date are summarized in Table 3. For **4b**/**4b′** and **II** the dynamic NMR results establish that the face exchange involves rate-limiting decomplexation of the olefin and is accompanied by fast inversion at the metal center (i.e., fast O-shift) in the olefin-dissociated intermediate, and that the anion is not involved. We presume that the face-exchange processes of **4a**/**4a′** and **I** are similar. Interestingly, in both the constrained geometry Ti series and the zirconocene series, the face-exchange barrier is higher for the more crowded examples. Several factors may influence the magnitude of the face-exchange barrier, including the metal−olefin bond strength, solvent involvement in the decomplexation of the olefin, and steric inhibition of chelate ring-opening. As a {η^5: η^1-$(C_5Me_4)SiMe_2N^tBu$}Ti(OR)$^+$ cation is expected to be less Lewis acidic than a {η^5: η^1-$(C_5H_4)SiMe_2NtBu$}Ti(OR)$^+$ cation, the Ti−olefin bond strength should be lower for **4b**/**4b′** than for **4a**/**4a′**. The fact that the face-exchange barriers follow the reverse trend suggests that other factors besides the Ti−olefin bond strength contribute to the face-exchange barriers. In both the constrained geometry Ti series and the zirconocene series, the activation entropies for the less crowded cases are ∼8−12 eu more negative than for the more crowded cases. While the differences are small, this trend suggests that solvent participation in the olefin decomplexation step may play a more important role in the less crowded cases. We are investigating the synthesis of nonchelated $L_nM(OR)(olefin)^+$ species to investigate these issues and to obtain more direct estimates of d^0 metal−olefin bond strengths.

Experimental Section

General Procedures. All experiments were carried out under purified nitrogen using a Vacuum Atmospheres glovebox or standard Schlenk techniques. Hydrocarbon solvents, diethyl ether, and tetrahydrofuran were distilled from Na/benzophenone. Chlorinated solvents were distilled from calcium hydride. All solvents were stored under N_2 prior to use. 2-Methyl-5-hexene-2-ol was prepared as described previously.[3a] $B(C_6F_5)_3$ (Boulder Scientific) was purified by double sublimation. $[Ph_3C][B(C_6F_5)_4]$ was obtained from Asahi Glass Co. and used as received. The Ti complexes {η^5: η^1-$C_5R_4SiMe_2N^tBu$}$TiMe_2$ (**1a,b**; R = H, Me) were prepared by literature procedures.[11a,b]

NMR spectra were recorded on Bruker AMX-600 (^{1}H), AMX-360 (^{1}H, ^{13}C, ^{11}B) or AC-300 (^{19}F) spectrometers, in Teflon-valved tubes

(30) The chemical shifts ($\delta_{observed}$, $\delta_{calculated}$) for the vinyl hydrogen resonances at 20 °C are as follows: H_{int}: 7.08, 7.10; H_{trans}: 5.11, 5.05; H_{cis}: 4.64, 4.61.

(31) The free energy of activation at the coalescence temperature determined using these parameters ($T_{coal} = -10$ °C; $\Delta G^{\ddagger}_{vinyl}$**4a**/**4a′** = 12.7-(3) kcal/mol) agrees well with the value (12.5(2) kcal/mol) estimated from the frequency difference between the unequal intensity H_{cis} doublets in the absence of exchange using the method of Shanan-Atidi, H.; Bar−Eli, K. H. *J. Chem. Phys.* **1970**, *74*, 961.

at ambient probe temperature (23 °C) unless otherwise indicated. NMR probe temperatures were controlled with a Bruker B-VT-1000E accessory coupled with a Eurotherm 818 controller calibrated versus a MeOH thermometer. Quoted temperatures are accurate to ±1 °C. ^{1}H and ^{13}C NMR chemical shifts were determined versus the solvent resonances and are reported relative to tetramethylsilane. ^{19}F and ^{11}B NMR chemical shifts are referenced to external $CFCl_3$ and external $BF_3{\cdot}Et_2O$, respectively. Coupling constants are reported in Hz. The NMR spectra of cationic complexes contain resonances for the free anions.[17,18] ^{1}H−^{1}H COSY and ^{13}C-detected ^{13}C−^{1}H phase-sensitive HETCOR spectra were acquired on the AMX-360 spectrometer and processed using standard Bruker programs. Detailed information on the ^{1}H 2D NOESY-EXSY experiments is provided below.

{η^5:η^1-$C_5H_4SiMe_2N^tBu$}$TiMe_2$ (1a): ^{1}H NMR (C_6D_6) δ 6.74 (t, J = 2.3, 2H, C_5H_4), 5.82 (t, J = 2.3, 2H, C_5H_4), 1.52 (s, 9H, ^{t}Bu), 0.65 (s, 6H, TiCH_3), 0.25 (s, 6H, SiCH_3). ^{13}C NMR (C_6D_6) δ 122.1 (d, J_{C-H} = 172, C_5H_4), 121.4 (d, J_{C-H} = 172, C_5H_4), 103.8 (s, CSiMe$_2$), 58.7 (s, CMe$_3$), 51.0 (q, J_{C-H} = 121, TiCH$_3$), 34.4 (q, J_{C-H} = 121, CMe_3), 0.9 (q, J_{C-H} = 120, SiCH$_3$).

{η^5:η^1-$C_5Me_4SiMe_2N^tBu$}$TiMe_2$ (1b): ^{1}H NMR (C_6D_6) δ 1.96 (s, 6H, C_5CH_3), 1.85 (s, 6H, C_5CH_3), 1.57 (s, 9H, ^{t}Bu), 0.51 (s, 6H, TiCH_3), 0.43 (s, 6H, SiCH_3). ^{13}C NMR (C_6D_6) δ 133.8 (s, C_5CH$_3$), 129.6 (s, C_5CH$_3$), 97.8 (s, CSiMe$_2$), 57.8 (s, CMe$_3$), 51.1 (q, J_{C-H} = 119, TiCH$_3$), 34.7 (q, J_{C-H} = 125, CMe_3), 15.1 (q, J_{C-H} = 125, C_5CH_3), 12.0 (q, J_{C-H} = 125, C_5CH_3), 6.3 (q, J_{C-H} = 119, SiCH$_3$).

{η^5-$C_5H_4SiMe_2NH^tBu$}$TiMe_2$(OCMe$_2$CH$_2$CH$_2$CH=CH$_2$) (2a) and {η^5:η^1-$C_5H_4SiMe_2N^tBu$}TiMe(OCMe$_2$CH$_2$CH$_2$CH=CH$_2$) (3a). Neat 2-methyl-5-hexene-2-ol (27 μL, 0.198 mmol) was added to a solution of **1a** (53.8 mg, 0.198 mmol) in C_6D_6 (2 mL) in a Teflon-valved NMR tube. The tube was shaken vigorously and maintained at 23 °C for 30 min. The color of the solution was bright yellow. ^{1}H and ^{13}C NMR spectra were obtained and revealed clean conversion of **1a** to a mixture of **2a** (95% NMR yield, determined using 1,4-$(SiMe_3)_2$−C_6H_4 as an internal standard) and **3a** (5% NMR yield). **2a**: ^{1}H NMR (C_6D_6) δ 6.37 (t, J = 2.4, 2H, C_5H_4), 6.09 (t, J = 2.4, 2H, C_5H_4), 5.87 (m, 1H, H_{int}), 5.11 (dq, J = 17.1, J = 1.8, 1H, H_{trans}), 5.01 (dm, J = 10.0, 1H, H_{cis}), 2.32 (m, 2H, CH_2), 1.75 (m, 2H, CH_2), 1.31 (s, 6H, OCMe$_2$), 1.09 (s, 9H, ^{t}Bu), 0.65 (s, 6H, TiCH_3), 0.34 (s, 6H, SiCH_3), NH signal obscured. ^{1}H NMR (CD_2Cl_2) δ 6.46 (t, J = 2.4, 2H, C_5H_4), 6.28 (t, J = 2.4, 2H, C_5H_4), 5.90 (m, 1H, H_{int}), 5.05 (dq, J = 17.1, J = 1.8, 1H, H_{trans}), 4.95 (dm, J = 10.0, 1H, H_{cis}), 2.33 (m, 2H, CH_2), 1.80 (m, 2H, CH_2), 1.42 (s, 6H, OCMe$_2$), 1.12 (s, 9H, ^{t}Bu), 0.76 (br s, 1H, NH), 0.30 (s, 6H, SiCH_3), 0.27 (s, 6H, TiCH_3). ^{13}C NMR (C_6D_6) δ 139.2 (d, J_{C-H} = 150, CH=), 126.1 (s, CSiMe$_2$), 118.6 (d, J_{C-H} = 172, C_5H_4), 115.9 (d, J_{C-H} = 172, C_5H_4), 114.5 (t, J_{C-H} = 155, CH$_2$=), 85.0 (s, OC), 49.7 (s, CMe$_3$), 47.8 (q, J_{C-H} = 122, TiCH$_3$), 44.1 (t, J_{C-H} = 126, CH$_2$), 33.8 (q, J_{C-H} = 125, CMe_3), 30.3 (q, J_{C-H} = 126, OCCH$_3$), 29.5 (t, J_{C-H} = 134, CH$_2$), 2.5 (q, J_{C-H} = 118, SiCH$_3$). **3a**: ^{1}H NMR (C_6D_6) δ 6.46 (m, 1H, C_5H_4), 6.32 (m, 1H, C_5H_4), 6.24 (m, 1H, C_5H_4), 1.34 (s, 9H, ^{t}Bu), 1.07 (s, 6H, OCMe$_2$), 0.61 (s, 3H, TiCH_3), 0.40 (s, 3H, SiCH_3), 0.37 (s, 3H, SiCH_3); the other signals overlap with those of **2a**.

{η^5-$C_5Me_4SiMe_2NH^tBu$}$TiMe_2$(OCMe$_2$CH$_2$CH$_2$CH=CH$_2$) (2b) and {η^5:η^1-$C_5Me_4SiMe_2N^tBu$}TiMe(OCMe$_2$CH$_2$CH$_2$CH=CH$_2$) (3b). A **2b**/**3b** mixture was generated from **1b** (43.7 mg, 0.137 mmol) in C_6D_6 (∼2 mL) and 2-methyl-5-hexene-2-ol (18.3 μL, 0.137 mmol) using the procedure described for **2a**/**3a**. The final solution was bright yellow. ^{1}H and ^{13}C NMR spectra were recorded and revealed clean conversion to **2b** (89% NMR yield vs internal standard) and **3b** (11% NMR yield). **2b**: ^{1}H NMR (C_6D_6) δ 5.90 (m, 1H, H_{int}), 5.15 (dq, J = 17.1, J = 1.8, 1H, H_{trans}), 5.02 (dq, J = 8.0, J = 1.8, 1H, H_{cis}), 2.34 (m, 2H, CH_2), 2.12 (s, 6H, C_5CH_3), 1.94 (m, 2H, CH_2), 1.88 (s, 6H, C_5CH_3), 1.47 (s, 6H, OCMe$_2$), 1.09 (s, 9H, ^{t}Bu), 0.47 (s, 6H, TiCH_3), 0.41 (s, 6H, SiCH_3). ^{1}H NMR (CD_2Cl_2) δ 5.89 (m, 1H, H_{int}), 5.05 (dm, J = 17.0, 1H, H_{trans}), 4.94 (dm, J = 10.0, 1H, H_{cis}), 2.32 (m, 2H, CH_2), 2.08 (s, 6H, C_5CH_3), 1.98 (s, 6H, C_5CH_3), 1.91 (m, 2H, CH_2), 1.51 (s, 6H, OCMe$_2$), 1.11 (s, 9H, ^{t}Bu), 0.57 (br s, 1H, NH), 0.28 (s, 6H, SiCH_3), 0.05 (s, 6H, TiCH_3). ^{13}C NMR (C_6D_6) δ 139.2 (d, J_{C-H} = 158, CH=), 129.2 (s, C_5CH$_3$), 127.2 (s, C_5CH$_3$), 119.9 (s, CSiMe$_2$), 114.4 (t, J_{C-H} = 155, CH$_2$=), 85.0 (s, OC), 49.9 (q, J_{C-H} = 121, TiCH$_3$), 49.6 (s, CMe$_3$), 44.6 (t, J_{C-H} = 127, CH$_2$), 33.7 (q, J_{C-H} = 125, CMe_3), 30.5 (q, J_{C-H} = 126, OCMe$_2$), 29.7 (t, J_{C-H} = 134, CH$_2$), 15.0 (q, J_{C-H} = 126, C_5CH_3), 11.9 (q, J_{C-H} = 126, C_5CH_3), 5.2 (q, J_{C-H} = 120, SiCH$_3$). **3b**: ^{1}H NMR (C_6D_6) δ 2.19 (s, 3H, C_5CH_3), 2.01 (s, 3H, C_5CH_3), 1.93 (s, 3H, C_5CH_3), 1.78 (s, 3H, C_5CH_3), 1.39 (s, 9H, ^{t}Bu), 1.23 (s, 6H, OCMe$_2$), 0.54 (s, 3H, SiCH$_3$), 0.52 (s, 3H, SiCH$_3$), 0.35 (s, 3H, TiCH$_3$); the other signals overlap with those of **2b**. {^{1}H}−^{13}C NMR (C_6D_6) δ 114.3 (CH$_2$=), 83.4 (OC), 49.6 (CMe$_3$), 44.5 (CH$_2$), 34.6 (CMe_3), 30.7 (OCCH$_3$), 29.3 (CH$_2$), 14.2 (C_5CH_3), 12.7 (C_5CH_3), 11.8 (C_5CH_3), 11.4 (C_5CH_3), 6.8 (SiCH$_3$), 6.5 (SiCH$_3$); the other signals overlap with those of **2b**.

[{η^5:η^1-$C_5H_4SiMe_2N^tBu$}Ti(OCMe$_2$CH$_2$CH$_2$CH=CH$_2$)][MeB(C_6F_5)$_3$] (4a/4a′).[32] A C_6D_6 solution of **2a**/**3a** (95/5) was prepared in an NMR tube as described above and concentrated under vacuum to give a dark, yellow-brown oil. The oil was cooled to −30 °C, and cold, solid $B(C_6F_5)_3$ (1 equiv vs **1a**) was added. The color of the oily mixture immediately turned brown-orange, and gas (CH_4) evolution was observed. The tube was rapidly cooled to −78 °C and C_6D_6 (∼2 mL) was added by vacuum transfer. The tube was slowly warmed to room temperature. The resulting biphasic mixture, consisting of a dark orange lower layer (ionic complexes) and a bright yellow upper layer (C_6D_6), was shaken vigorously and maintained at room temperature until gas evolution ceased (∼15−30 min). The upper benzene layer was removed by pipet, and the remaining oil was dried under vacuum. The gummy residue was dissolved in CD_2Cl_2 to give a clear, bright orange solution. NMR analysis established the formation of **4a** (44% yield vs internal standard) and **4a′** (27% yield). **4a**: ^{1}H NMR (CD_2Cl_2, −60 °C) δ 7.02 (m, 1H, H_{int}), 6.87 (m, J = 2.3, 1H, $C_5H_4^d$), 6.78 (m, J = 1.2, 1H, $C_5H_4^c$), 6.57 (m, J = 1.6, 1H, $C_5H_4^b$), 6.34 (m, J = 2.0, 1H, $C_5H_4^a$), 5.06 (d, ^3J = 18.4, 1H, H_{trans}), 4.78 (d, ^3J = 10.8, 1H, H_{cis}), 2.51 (m, 2H, CH_2), 2.20 (m, 2H, CH_2), 1.32 (s br, 6H, OC(CH_3)$_2$), 1.24 (s, 9H, ^{t}Bu), 0.73 (s, 3H, SiCH_3^b), 0.58 (s, 3H, SiCH_3^a). ^{13}C NMR (CD_2Cl_2, −60 °C) δ 159.4 (d, J_{C-H} = 155, =CH), 124.8 (d, J_{C-H} = 172, $C_5H_4^a$), 123.9 (d, J_{C-H} = 172, $C_5H_4^b$), 122.6 (d, J_{C-H} = 172, $C_5H_4^d$), 119.4 (d, J_{C-H} = 172, $C_5H_4^c$), 113.4 (s, CSiMe$_2$), 104.3 (t, J_{C-H} = 159, CH$_2$=), 90.3 (s, OC), 66.5 (s, CMe$_3$), 49.3 (t, J_{C-H} = 130, CH$_2$), 33.2 (q, J_{C-H} = 128, CMe_3), 31.6 (t, J_{C-H} = 128, CH$_2$), 30.2 (q, J_{C-H} = 129, OCCH$_3^b$), 26.5 (q, J_{C-H} = 129, OCCH$_3^a$), −0.6 (q, J_{C-H} = 120, SiCH$_3^a$), −0.85 (q, J_{C-H} = 120, SiCH$_3^b$). **4a′**: ^{1}H NMR (CD_2Cl_2, −60 °C) δ 7.24 (m, 1H, H_{int}), 6.73 (m, J = 1.6, 1H, $C_5H_4^d$), 6.66 (2m, J = 2.0, 2H, $C_5H_4^{b,c}$), 6.55 (m, J = 2.3, 1H, $C_5H_4^a$), 5.04 (d, ^3J = 18.4, 1H, H_{trans}), 4.32 (d, ^3J = 10.8, 1H, H_{cis}), 2.51 (m, 2H, CH_2), 2.20 (m, 2H, CH_2), 1.35 (s, 3H, OCCH_3^b), 1.30 (s, 3H, OCCH_3^a), 1.18 (s, 9H, ^{t}Bu), 0.72 (s, 3H, SiCH_3^b), 0.64 (s, 3H, SiCH_3^a). ^{13}C NMR (CD_2Cl_2, −60 °C) δ 163.1 (d, J_{C-H} = 151, CH=), 125.9 (d, J_{C-H} = 172, $C_5H_4^a$), 123.0 (d, J_{C-H} = 172, $C_5H_4^b$), 121.7 (d, J_{C-H} = 172, $C_5H_4^d$), 119.9 (d, J_{C-H} = 172, $C_5H_4^c$), 114.1 (s, CSiMe$_2$), 98.0 (t, J_{C-H} = 159, CH$_2$=), 90.5 (s, OC), 63.1 (s, CMe$_3$), 48.8 (t, J_{C-H} = 130, CH$_2$), 33.0 (q, J_{C-H} = 128, CMe_3), 32.3 (t, J_{C-H} = 129, CH$_2$), 30.8 (OCCH$_3^a$), 28.7 (q, J_{C-H} ≈ 131, OCCH$_3^b$), −0.4 (q, J_{C-H} = 120, SiCH$_3^b$), −0.86 (q, J_{C-H} = 120, SiCH$_3^a$).

[{η^5:η^1-$C_5Me_4SiMe_2N^tBu$}Ti{OCMe$_2$CH$_2$CH$_2$CH=CH$_2$}][MeB(C_6F_5)$_3$] (4b/4b′).[32] This compound was generated from a **2b**/**3b** mixture (89/11) and 1 equiv of $B(C_6F_5)_3$ using the procedure described for **4a**/**4a′**. NMR analysis revealed that **2b**/**3b** underwent conversion to **4b** (67% yield vs internal standard) and **4b′** (22% yield). **4b**: ^{1}H NMR (CD_2Cl_2, −20 °C) δ 6.52 (m, 1H, H_{int}), 4.99 (d, ^3J = 18.4, 1H, H_{trans}), 4.45 (dd, ^3J = 8.6, ^2J = 2.5, 1H, H_{cis}), 2.53 (m, 2H, CH_2^b), 2.25 (m, 2H, CH_2^a), 2.22 (s, 3H, $C_5CH_3^d$), 2.18 (s, 3H, $C_5CH_3^c$), 2.13 (s, 3H, $C_5CH_3^b$), 2.03 (s, 3H, $C_5CH_3^a$), 1.43 (s, 3H, OCCH_3^b), 1.41 (s, 3H, OCCH_3^a), 1.31 (s, 9H, ^{t}Bu), 0.87 (s, 3H, SiCH_3^b), 0.79 (s, 3H, SiCH_3^a). ^{13}C NMR (CD_2Cl_2, −60 °C) δ 162.8 (d, J_{C-H} = 152, CH=), 138.5 (s, C_5CH$_3$), 136.5 (s, C_5CH$_3$), 135.8 (s, C_5CH$_3$), 133.2 (s, C_5CH$_3$), 109.3 (s, CSiMe$_2$), 106.0 (t, J_{C-H} = 157, CH$_2$=), 90.2 (s, OC), 64.7 (s, CMe$_3$), 49.4 (t, J_{C-H} = 122, CH$_2^a$), 33.5 (q, J_{C-H} = 127, CMe_3), 31.5 (t, J_{C-H} = 134, CH$_2^b$), 31.0 (q, J_{C-H} = 124, OCCH$_3^b$), 27.8 (q, J_{C-H} = 128, OCCH$_3^a$), 15.0 (q, J_{C-H} = 128, $C_5CH_3^a$), 14.8 (q, J_{C-H} = 128, $C_5CH_3^d$), 13.1 (q, J_{C-H} = 128, $C_5CH_3^b$), 12.2 (q, J_{C-H} = 128, $C_5CH_3^c$), 5.1 (q, J_{C-H} = 121, SiCH$_3^a$), 4.2 (q, J_{C-H} = 121, SiCH$_3^b$). **4b′**: ^{1}H NMR (CD_2-

(32) The superscript labels (a, b, c, d) following the ^{1}H and ^{13}C chemical shift assignments of **4a**/**4a′** and **4b**/**4b′** denote resonances that are correlated in ^{13}C−^{1}H HETCOR spectra.

Cl_2, −20 °C) δ 7.30 (m, 1H, H_{int}), 4.56 (dt, ^3J = 17.6, ^2J = 2.5, 1H, H_{trans}), 4.01 (dd, ^3J = 9.4, ^2J = 2.9, 1H, H_{cis}), 2.60 (m, 2H, CH_2), 2.25 (m, 2H, CH_2), 2.24 (s, 3H, C_5CH_3[d]), 2.14 (s, 3H, C_5CH_3[c]), 2.11 (s, 3H, C_5CH_3[b]), 2.07 (s, 3H, C_5CH_3[a]), 1.41 (s, 3H, OCCH_3[b]), 1.33 (s, 3H, OCCH_3[a]), 1.28 (s, 9H, ^{t}Bu), 0.91 (s, 3H, SiCH_3[b]), 0.71 (s, 3H, SiCH_3[a]). ^{13}C NMR (CD_2Cl_2, −60 °C) δ 167.8 (d, J_{C-H} = 155, *C*H═), 108.6 (s, *C*SiMe$_2$), 101.6 (t, J_{C-H} = 157, *C*H$_2$═), 90.1 (s, O*C*), 63.7 (s, *C*Me$_3$), 49.3 (t, J_{C-H} = 122, *C*H$_2$), 33.3 (q, J_{C-H} = 127, C*Me*$_3$), 29.7 (2 s, OC(*C*H$_3$)$_2$), 15.5 (q, J_{C-H} = 128, C_5CH_3[c]), 15.0 (overlaps with a resonance of the major diastereomer, C_5CH_3[d]), 13.4 (q, J_{C-H} = 128, C_5CH_3[a]), 12.1 (q, J_{C-H} = 129, C_5CH_3[b]), 5.2 (q, J_{C-H} = 120, SiCH_3[b]), 4.4 (q, J_{C-H} = 119, SiCH_3[a]); the other Cp signals overlap with anion resonances.

[{η^5:η^1-$C_5Me_4SiMe_2N^tBu$}Ti(OCMe$_2$CH$_2$CH$_2$CH═CH$_2$)][B(C$_6$F$_5$)$_4$] (5b/5b′). This compound was generated by the procedure described for **4b**/**4b′** using a 89:11 mixture of **2b**/**3b** (0.082 mmol) and 1 equiv of [Ph_3C][$B(C_6F_5)_4$]. The variable-temperature ^{1}H and ^{13}C spectra revealed that **5b**/**5b′** are formed in the same yield and ratio as **4b**/**4b′** (**5b**: 67% yield vs internal standard; **5b′**: 22%) and that the dynamic behavior of **5b**/**5b′** is identical to that of **4b**/**4b′**. The spectra of **5b**/**5b′** are identical to those of **4b**/**4b′** except for the anion and Ph_3CCH_3 resonances.

[{η^5:η^1-$C_5H_4SiMe_2N^tBu$}Ti(OCMe$_2$CH$_2$CH$_2$CH═CH$_2$)(THF)][MeB(C$_6$F$_5$)$_3$] (6a). Excess THF (50 μL, 0.60 mmol) was added to a solution of **4a**/**4a′** (.∼0.1 mmol) in CD_2Cl_2 (∼2 mL). The color of the solution changed rapidly from bright orange to yellow-orange. The reaction mixture was stirred for 10 min, the volatiles were removed under vacuum, and CD_2Cl_2 (∼2 mL) was added by vacuum transfer. This procedure was repeated a second time. NMR spectra were recorded and revealed that **4a**/**4a′** was completely converted to **6a**. **6a**: ^{1}H NMR δ 7.19 (m, 1H, C_5H_4), 6.70 (m, 2H, C_5H_4), 6.26 (m, 1H, C_5H_4), 5.82 (m, 1H, H_{int}), 5.05 (dd, J = 17.3, J = 2.2, 1H, H_{trans}), 4.98 (dd, J = 10.0, J = 2.2, 1H, H_{cis}), 4.05 (m, 2H, THF), 3.93 (m, 2H, THF), 2.2−2.0 (m, 6H, THF and CH_2−CH═), 1.43 (s, 3H, OCCH_3), 1.42 (s, 3H, OCCH_3), 1.31 (s, 9H, ^{t}Bu), 0.72 (s, 3H, SiCH_3), 0.68 (s, 3H, SiCH_3). ^{13}C NMR: δ 137.6 (d, J_{C-H} = 154, *C*H═), 125.8 (d, J_{C-H} = 175, C_5H_4), 123.7 (d, J_{C-H} = 175, C_5H_4), 123.0 (d, J_{C-H} = 175, C_5H_4), 122.1 (d, J_{C-H} = 175, C_5H_4), 115.4 (t, J_{C-H} = 156, *C*H$_2$═), 112.9 (s, *C*SiMe$_2$), 92.5 (s, O*C*), 79.3 (t, J_{C-H} = 153, OCH$_2$ THF), 64.1 (s, *C*Me$_3$), 44.3 (t, J_{C-H} = 130, *C*H$_2$−CH), 30.4 (q, J_{C-H} = 127, OC*C*H$_3$), 29.9 (t, J_{C-H} = 128, *C*H$_2$), 29.7 (t, J_{C-H} = 132, *C*H$_2$ THF), 0.6 (q, J_{C-H} = 121, Si*C*H$_3$), −0.1 (q, J_{C-H} = 121, Si*C*H$_3$).

[{η^5:η^1-$C_5Me_4SiMe_2N^tBu$}Ti(OCMe$_2$CH$_2$CH$_2$CH═CH$_2$)(THF)][B(C$_6$F$_5$)$_4$] (6b). Compound **6b** was generated from **5b**/**5b′** using the procedure described for **6a**. **6b**: ^{1}H NMR (CD_2Cl_2) δ 5.84 (m, 1H, H_{int}), 5.06 (dd, J = 17.3, J = 2.2, 1H, H_{trans}), 5.00 (dd, J = 10.0, J = 2.2, 1H, H_{cis}), 4.05 (m, 2H, THF), 3.95 (m, 2H, THF), 2.33 (s, 3H, C_5CH_3), 2.24 (s, 3H, C_5CH_3), 2.09 (s, 3H, C_5CH_3), 2.05 (s, 3H, C_5CH_3), 2.2−2.0 (m, 4H, THF), 1.46 (s, 3H, OCCH_3), 1.45 (s, 3H, OCCH_3), 1.34 (s, 9H, ^{t}Bu), 0.81 (s, 3H, SiCH_3), 0.79 (s, 3H, SiCH_3); resonances of Ph_3CCH_3 were also observed.

Molecular Modeling. Molecular mechanics calculations were performed using the software package *Cerius*^{2} (version 2.1, Molecular Simulations, Inc.). The universal force field (UFF) developed by Rappé was used.[33] The parameters used to generate the UFF include a set of hybridization-dependent atomic bond radii, a set of hybridization angles, van der Waals parameters, torsional and inversion barriers, and a set of effective nuclear charges. The {η^5: η^1-$C_5Me_4SiMe_2N^tBu$}Ti unit was constructed and constrained to atomic coordinates taken from crystallographic data for {η^5: η^1-$C_5Me_4SiMe_2N^tBu$}$TiCl_2$ (centroid-Ti−N angle = 108°).[11c] Constraints were implemented by the "Open Force Field Setup-Energy Terms-Restraints" package. The Ti−O−C angle was constrained to 160°, and the Ti−C distances were constrained to Ti−C_{int} = 2.70 Å, Ti−C_{ter} = 2.55 Å, based on crystallographic data for **I** and **II**. No other constraints were applied. The structure was minimized by conjugate gradient methods to a 0.1 kcal mol^{-1} Å^{-1} root-mean-square force. Different conformations of the alkoxide−olefin chelate ring were examined to find a global energy minimum for each diastereomer. The angles between Ti−C−C and CH_2═CH− planes for the lowest-energy structures are 78° for the *R*,*R*-diastereomer and 88° for the *R*,*S*-diastereomer.

NMR Simulations for 4b/4b′. Simulations were performed using the software package gNMR (Cherwell Scientific, version 3.6.5). The vinyl region was simulated as a set of three two-site exchange systems. The chemical shifts and coupling constants for the three vinyl hydrogens of each diastereomer in the slow limit exchange (below −40 °C) were used to set up the spin systems of the two species, and the relative population ratio was fixed at 75/25. The natural line width in the absence of exchange (W_0 = 1.4 Hz) was measured at −40 °C for H_{cis}^A and H_{cis}^B and confirmed by observation of the same line width at −60 °C. The accuracy of the NMR parameters and population ratio was assessed by comparison of the simulated spectrum with the experimental spectrum at −40 °C. Then, spectra were calculated assuming that exchange of each pair of corresponding hydrogens, H_{int}^A/H_{int}^B, H_{trans}^A/H_{trans}^B, and H_{cis}^A/H_{cis}^B, occurs at the same rate, which was optimized to match the simulated and experimental spectra. The uncertainties in the exchange rate constants determined in this manner are ∼± 20%. Activation parameters were determined by a standard Eyring analysis (Figure 4). The standard deviations for the least-squares fit were used to estimate the uncertainties in $\Delta H^{\ddagger}_{vinyl}{}^{AB}$ and $\Delta S^{\ddagger}_{vinyl}{}^{AB}$.

The Si−*Me* region was simulated as a four-site system (A1, A2, B1, B2) in 3/8:3/8:1/8:1/8 relative population ratio. The chemical shifts observed in the slow-limit exchange (below −5 °C) were used to set up the spin system using a natural line width W_0 = 1.4 Hz. The chemical shifts of the Si−*Me* resonances vary slightly with temperature between −5 and 10 °C (δ $SiMe_{A1}$ 0.788 to 0.792; $SiMe_{A2}$ 0.875 to 0.890; $SiMe_{B1}$ 0.712 to 0.720; $SiMe_{B2}$ 0.910 to 0.915); chemical shifts in the absence of exchange at higher temperatures were estimated by linear extrapolation of the −5 to 10 °C values. Spectra were simulated as described in the text, assuming that the six possible site-to-site exchanges (A1−A2, A1−B1, A1−B2, A2−B1, A2−B2, B1−B2) occur at relative rates of 9/3/3/3/3/1. Exchange rates were obtained by comparison of experimental spectra with simulated spectra for eight temperatures in the range −5−60 °C. As shown in Figure 3, a good fit was obtained using this procedure. The uncertainty in the Si−*Me* site-to-site exchange rates was probed by extensive simulations using different values for R_{A1A2}, R_{AxBy}, and R_{B1B2}.

Variable-Temperature ^{1}H 2D-EXSY NMR Spectra of 4b/4b′. Two-dimensional ^{1}H spectra were obtained using the Bruker AMX-360 spectrometer with the program "noesysh". The pulse sequence was D1-90°−D0-90°−D9-90°-FID. The initial relaxation delay time D1 was typically 3 s (>4 × T_1, vide infra), the initial D0 was 3 μs, and the mixing time D9 (τ_m) was varied according to the experimental temperature (vide infra). The pulse sequence was repeated for 128 values of D0, that is, the F_1 dimension contained 128 points, which was then zero-filled to 512 points. The F_2 dimension contained 2048 points. The number of scans per experiment was 16, giving a total experiment time of ∼135 min. The optimal mixing time $\tau_{m,opt}$ was chosen on the basis of eq 11 to minimize the relative error in the rate constant.[34,35] The activation parameters determined from the Eyring analysis of the line-shape data (Figure 4) were used to estimate rate constants k_{AB} and k_{BA}. Spin−lattice relaxation times T_1 were measured by using the standard inversion−recovery method. T_1 values for the vinyl hydrogens of **4b**/**4b′** (A/B) measured at 0 and −20 °C are listed in Table 4.

$$\tau_{m,opt} \sim 1/(T_1^{-1} + k_{AB} + k_{BA}) \qquad (11)$$

Control experiments established that EXSY-determined rate constants are not significantly affected by a ±50% variation in $\tau_{m,opt}$. Uncertainties in rate constant values were estimated assuming ±1% uncertainty in the finite *S*/*N* ratios of the computed spectra, and ±2% uncertainty in

(33) (a) Rappé, A. K.; Casewitt, C. J.; Colwell, K. S.; Goddard, W. A., III; Skiff, W. M. *J. Am. Chem. Soc.* **1992**, *114*, 10024. (b) Rappé, A. K.; Colwell, K. S.; Casewitt, C. J. *Inorg. Chem.* **1993**, *32*, 3438.

(34) The mixing time must be of sufficient magnitude to give relatively strong cross-peaks but not so long that the signal intensities become insensitive to exchange rates, or all signals lose appreciable intensity due to spin−lattice relaxation.

(35) Abel, E. W.; Coston, T. P. J.; Orrell, K. G.; Sik, V.; Stephenson, D. *J. Magn. Res.* **1986**, *70*, 34.

Table 4. T_1 Values for the Vinyl Hydrogens of **4b**/**4b′** at 0 and −20 °C

T, °C	H_{int}^A	H_{int}^B	H_{trans}^A	H_{trans}^B	H_{cis}^A	H_{cis}^B
0	0.85	0.85	0.60	0.50	0.50	0.50
−20	0.60	0.55	0.40	0.35	0.35	0.35

2D signal integrations. Two separate experiments performed at −30 °C gave results consistent with the uncertainty estimated using these assumptions.

Acknowledgment. This work was supported by NSF grant CHE-9413022 (R.F.J.). J.-F.C. thanks the French "Centre National de la Recherche Scientifique" and Elf Atochem for support.

Supporting Information Available: NMR spectra of **4b**/**4b′** and **4a**/**4a′** (PDF). This material is available free of charge via the Internet at http://pubs.acs.org.

JA003209L